

# THE BHB STARS IN THE SURVEY FIELDS OF RODGERS ET AL. (1993): NEW OBSERVATIONS AND COMPARISONS WITH OTHER RECENT SURVEYS.

T.D.KINMAN<sup>1</sup>

NOAO, P.O.Box 26732, Tucson, Arizona 85726, USA

WARREN R. BROWN

Smithsonian Astrophysical Observatory, 60 Garden St., Cambridge, MA 02138, USA

*Accepted in AJ*

## ABSTRACT

We study blue horizontal branch (BHB) and RR Lyrae stars in the Rogers et al. (1993a) fields and compare their velocity and density distributions with other surveys in the same part of the sky. Photometric data are given for 176 early-type stars in the northern field. We identify fourteen BHB stars and four possible BHB stars, and determine the selection efficiency of the *Century* Survey, the *HK* Survey, and the *SDSS* survey for BHB stars. We give light curves and  $\gamma$  radial velocities for three type *ab* RR Lyrae stars in the northern field; comparison with the nearby *LONEOS* Survey shows that there is likely to be an equal number of lower-amplitude type *ab* RR Lyrae stars that we do not find. There are therefore at least *twice* as many BHB stars as type *ab* RR Lyrae stars in the northern field — similar to the ratio in the solar neighborhood. The velocity distribution of the southern field shows no evidence for an anomalous thick disk that was found by Gilmore et al. (2002); the halo velocity peaks at a slightly prograde rotational velocity but there is also a significant retrograde halo component in this field. The velocity distribution in the northern field shows no evidence of Galactic rotation for  $|Z| \geq 4$  kpc and a slight prograde motion for  $|Z| < 4$  kpc. The space densities of BHB stars in the northern field agree with an extrapolation of the power-law distribution recently derived by de Propris et al. (2010). For  $|Z| < 4$  kpc, however, we observe an excess of BHB stars compared with this power-law. We conclude that these BHB stars mostly belong to a spatially flattened, non-rotating inner halo component of the Milky Way in confirmation of the Kinman et al. (2009) analysis of *Century* Survey BHB stars.

*Subject headings:* stars: horizontal branch, Galaxy: structure, Galaxy: halo

## 1. INTRODUCTION

In this paper we identify blue horizontal branch (BHB) and RR Lyrae stars among the 176 early type stars in the Rodgers et al. (1993a) fields and compare their velocity and density distributions with those of other surveys in the same part of the sky. BHB and RR Lyrae stars are interesting because they are luminous tracers of the old stellar population. Our targets come from Rodgers et al. (1993a), who used the Anglo-Australian Observatory Schmidt Telescope to make an objective-prism survey ( $600 \text{ \AA mm}^{-1}$  at  $H\gamma$ ) in two  $70 \text{ deg}^2$  fields:  $l = 90^\circ, b = -45^\circ$  in the North (hereafter *NR*) and  $l = 270^\circ, b = -45^\circ$  in the South (hereafter *SR*). They determined spectral types using the relative strengths of the CaII K-line and the  $H\delta$  Balmer line for stars in the magnitude range  $10 < V < 15.5$ . They obtained follow-up coude spectra ( $2.4 \text{ \AA}$  resolution) of 332 of these stars at the Mt. Stromlo 74-inch telescope. The resulting sample of high Galactic latitude *metal-rich* stars are discussed in Rodgers et al. (1993b), an extension of Rodgers (1971). The sample of *metal-weak* stars is discussed in Rodgers et al. (1993c); they conclude that this sample contains BHB stars but do not identify these stars individually.

We use photometry and spectroscopy to determine the stellar nature of the BHB and RR Lyrae candidates given

by Rodgers et al. (1993c). BHB stars can be identified with considerable certainty, for example, by using a  $(B - V)$  vs  $(u - B)_K$  plot (Kinman et al. 1994). *GALEX* ultraviolet magnitudes can also be used to identify BHB stars (Kinman et al. 2007b). Rodgers et al. (1993a) give no colors for their stars, only  $V$  magnitudes calculated from the *Hubble Space Telescope* (*HST*) Guide Star Catalog (Lasker et al. 1990). We therefore obtain  $V$ ,  $(B - V)$  and  $(u - B)_K$  photometry for most of the stars of spectral type A8 and earlier in the *NR* field. Photometry is also taken from the 2MASS and *GALEX* catalogs. In addition, the *NR* field is covered by the Northern Sky Variability Survey (hereafter *NSVS*; Wózniański et al. 2004) and the *ASAS-3* variability survey (Pojmański, 2002). We use these two surveys to study variability among the early-type stars and identify possible new RR Lyrae stars. We obtain  $V$  light-curves and phase-corrected radial velocities for the three brightest RR Lyrae stars in the *NR* field.

The radial velocity distribution of the stars is important because the *NR* and *SR* fields have Galactic longitudes for which the sight-line component of Galactic rotation is the greatest and thus for which radial velocity can distinguish between disk and halo populations. An additional constraint on the nature and origin of the BHB and RR Lyrae stars is provided by their spatial distribution. We combine our photometry and luminosity estimates to make accurate distance estimates and

<sup>1</sup> The NOAO are operated by AURA, Inc. under cooperative agreement with the National Science Foundation.

establish that most of these stars belong to a flattened, non-rotating inner halo component of the Milky Way.

### 1.1. Comparison with Other Surveys

Gilmore et al. (2002) obtained radial velocities for  $\sim 2000$  main sequence *turn-off* stars in two southern fields, one of which is coincident with (but smaller) than the *SR* field. The distribution of radial velocities in the Gilmore et al. fields showed a thick disk that had an unusually low galactic rotation at a few kpc above the plane; their data was also “suggestive of a retrograde halo stream”. They concluded that their sample was dominated by stars from a disrupted satellite that had merged with the disk of the Milky Way some 10 to 12 Gyr ago. Navarro et al. (2004) suggested that these kinematically anomalous thick disk stars are connected with the metal-poor high-velocity “Arcturus Group” in the solar neighborhood. Carollo et al. (2010) have also identified a disk population with an anomalously low rotation (the metal-weak thick disk) and noted its similarity to the population found by Gilmore et al.<sup>2</sup> A broader discussion of these streams has been given by Minchev et al. (2009).

Our main interest in this paper is the *NR* field, which is overlapped by and/or contiguous with a number of recent surveys. Stripes 76 and 79 of the Seventh Data Release (*DR7*) of the Sloan Digital Sky Survey (*SDSS*) (Abazajian et al. 2009) cross the *NR* field and contain 33 stars whose positions coincide with those listed in the *NR* field, but only 8 of these (roughly those with  $V \geq 14.5$ ) are faint enough to have reliable *SDSS* photometry<sup>3</sup>. Smith et al. (2010) have given probabilities that a star is a BHB star for 27,074 stars in the *DR7* of the *SDSS*; five of our candidate BHB stars in the *NR* field are included in their catalog. The *NR* field is also contiguous to the *SDSS* Stripe 82 which has been searched for RR Lyrae stars, subdwarfs and BHB stars by Watkins et al. (2009), Smith et al. (2009) and Deason et al. (2010) respectively. These studies and that of Belokurov et al. (2007) show that the *NR* field is unlikely to be affected by the Hercules-Aquila Cloud (the nearest large sub-structure in the halo).

The two surveys most relevant to our study are the *HK* Survey and the *Century* Survey. Beers et al. (2007b) (hereafter *B2M*) used 2MASS colors to assign “High”, “Medium” or “Low” probabilities that the stars of the *HK* Survey (Beers et al. 1988, 1996) are BHB stars. The *B2M* survey overlaps  $\sim 50\%$  of the area of the *NR* survey. In this overlap region they list 45 stars; 28 of these were given by Rodgers et al. (1993a) and which we include in our list of BHB candidates (Table 5). The 17 stars not listed by Rodgers et al. are given separately in Table 10 in Appendix B; these are mostly stars that are either too red or too faint to have been included in the *NR* survey. The Century Halo Star Survey (Brown et al. 2004, 2008) (hereafter *CHSS*) overlaps  $\sim 30\%$  of the *NR* field and has 12 stars in this area<sup>4</sup>. Ten are listed

by Rodgers et al. (1993a). The other two have  $V > 15.0$  and thus are fainter than the limit at which the *NR* survey is complete. Both the *B2M* and *CHSS* surveys use 2MASS colors to select BHB candidates but since the *CHSS* additionally uses slit spectra (2.3 Å resolution,  $\lambda\lambda$  3450–5450 Å), it is much more effective in identifying these stars.

Spectra are already available for 18 of the stars in the *NR* field; they were obtained with the RC spectrograph at the 4m Mayall telescope at Kitt Peak ( $\sim 0.8$  Å resolution,  $\lambda\lambda$  3880–4580 Å). We are grateful to Dr. Nick Suntzeff (priv. communication 1996, 1998) for making available the radial velocities from these spectra. Additional spectra for this study were obtained with the FAST spectrograph of the Whipple 1.5-m telescope (2.3 Å resolution,  $\lambda\lambda$  3600–5500 Å).

### 2. PHOTOMETRY OF STARS IN THE *NR* FIELD.

We first consider the photometry of the stars in the *NR* field. We give photometric data for 176 stars in the Northern field of Rodgers et al. (1993) in Table 1 (at end of paper). New photometry is given for 105 of these stars; Johnson *B*, *V* photometry is taken from the literature for 7 others.

Our new photometric observations were made with the KPNO 0.9-m telescope between August 1996 and December 1997, inclusive. The detector was a  $512 \times 512$  Tektronix chip under control of the *CCDPHOT* program (Tody & Davis, 1992). The measurements were made in a  $128 \times 128$  pixel area at the center of the chip. This  $90 \times 90$  arcsec area was small enough to allow a rapid readout and yet large enough for acquisition to be easy. The filter slide was under computer control so that the observations could be made with an assigned integration time for each filter and this cycle could be repeated for a chosen number of times. Bias and flat-field observations were made in the usual way and used by the program to compute instrumental magnitudes that were immediately available at the end of each integration cycle. Thus, the approximate magnitude and color of the star were available immediately after each integration cycle. The integrations through the various filters were made in rapid succession and so the colors were relatively unaffected by slow trends in the transparency. We concentrated on the stars with spectral types earlier than A8. One or two integration cycles with the *CCDPHOT* program were sufficient to decide whether a star had the appropriate (*B* – *V*) color for a BHB star; if it had, the observations were continued.

The *V*, *B* – *V* and (*u* – *B*)<sub>K</sub> observations were made as described in Kinman et al. (1994). We used the *B*, *V* standards of Landolt (1992) — primarily those in SA-114 and SA-115. For (*u* – *B*)<sub>K</sub>, the following secondary standards near the Rodgers field were used: HD 2857 (2.094); BD +02–0089 (1.938); BD +00–0145 (1.831); SA 114–750 (1.952); SA 115–271 (1.918); SA 115–420 (1.924). The adopted value of (*u* – *B*)<sub>K</sub> is given in parentheses following the name of each star. We measured the Strömgren *H*β index for 30 of the brighter program stars ( $V < 14$ ) using well-observed early-type stars taken from Stetson (1991) as standards. The *E*(*B* – *V*) correction

$12.5 < J < 15.5$ ,  $-0.20 < (J - H) < 0.10$  and  $-0.10 < (H - K) < 0.10$ . Spectroscopic analysis showed that 47% of these were BHB stars.

<sup>2</sup> The analysis of Carollo et al. (2010) has, however, been criticized by Schönrich et al. (2010).

<sup>3</sup> The BHB star surveys by Xue et al. (2008) and Brown et al. (2010) that are based on the *DR6* of the *SDSS* do not include stars from the *NR* field.

<sup>4</sup> This survey used the 2MASS survey to extract stars with

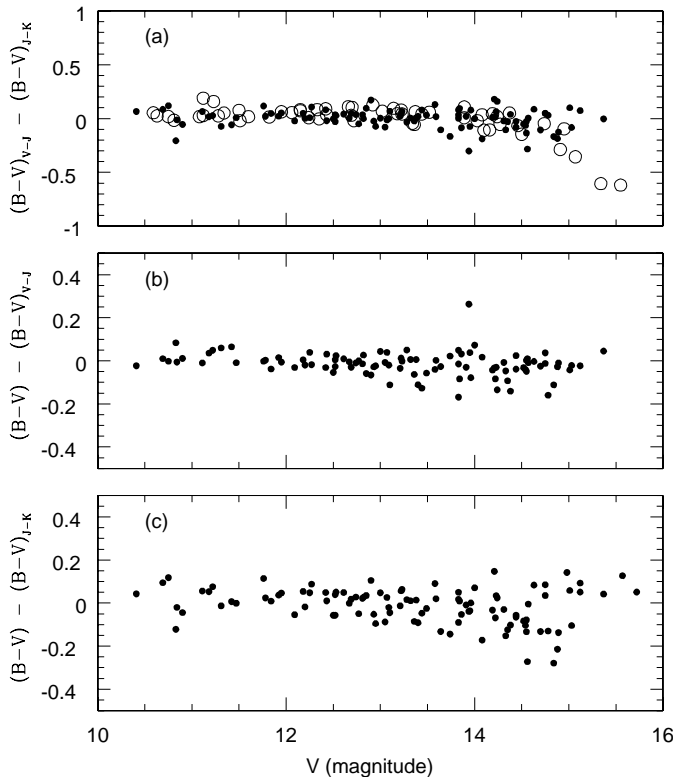


FIG. 1.— (a) The difference between the  $(B-V)$  calculated from  $(V-J)$  and that from  $(J-K)$  vs.  $V$  magnitude. The filled circles are for the calibrating stars (with known  $(B-V)$ ). The open circles are for stars whose  $(B-V)$  was not observed. (b) The difference between the observed  $(B-V)$  and that calculated from  $(V-J)$  vs.  $V$  magnitude. (c) The difference between the observed  $(B-V)$  and that calculated from  $(J-K)$  vs.  $V$  magnitude.

for galactic extinction given in col. 7 of Table 1 is from Schlegel et al. (1998). We assumed  $A(V) = 3.1 \times E(B-V)$  and  $A(u-B)_K = 0.89 \times E(B-V)$  (Kinman et al. 1994).

Our mean  $V$ ,  $B-V$  and  $(u-B)_K$  for the program stars are given with their *rms* errors in cols. 3, 4 and 5 of Table 1. A  $V$  magnitude that has no error and a superscript <sup>a</sup> is taken from the *ASAS-3* catalog (Pojmański 2002). A  $V$  with a superscript <sup>b</sup> is a mean of the magnitudes given in the *ASAS-3* catalog and the *GSC-2.3* catalog (Lasker et al. 2008). The sources of the other  $V$  magnitudes are given in the table notes.

The *GALEX* *NUV* magnitudes (col. 8) are taken from *MAST* (The Multimission Archive at STScI, <http://archive.stsci.edu/>). *NUV* is a near-UV magnitude (effective wavelength 2267 Å) that can be used to select BHB stars (Kinman et al. 2007b). The  $J$  and  $K$  magnitudes are taken from the 2MASS Point Source Catalog using the *Vizier* access tool. The  $m_R$  red magnitude (col. 11) and its scatter ( $\Sigma_{mR}$ ) (col. 12) were taken from the Northern Sky Variability Survey (Woźniak et al. 2004).

We also calculated  $(B-V)_0$  from both  $(V-J)_0$  and from  $(J-K)_0$  using the following relations that were derived from the program stars with known  $(B-V)$ :

$$(B-V)_0 = 0.588 \pm 0.022 \times (V-J)_0 - 0.041 \pm 0.011 \quad (1)$$

$$(B-V)_0 = 1.553 \pm 0.084 \times (J-K)_0 + 0.031 \pm 0.013 \quad (2)$$

Brown et al. (2008) derived  $(B-V)_0$  from Balmer line

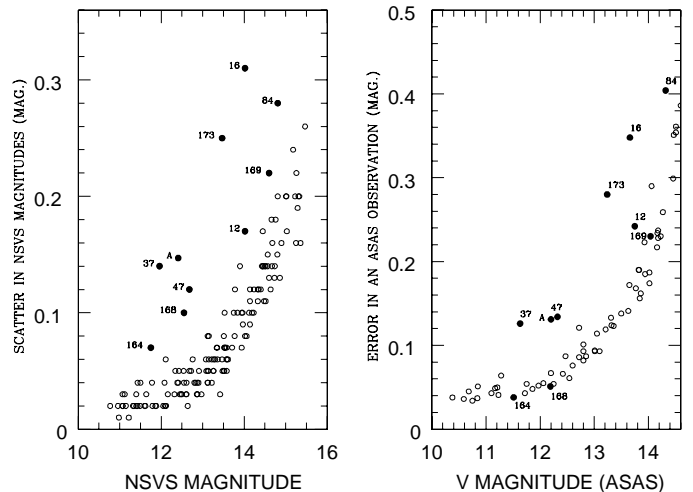


FIG. 2.— (Left) The scatter ( $\Sigma_{mR}$ ) in the individual *NSVS* magnitudes ( $m_R$ ) (ordinate) vs.  $m_R$ . (Right) The error of a single  $V$  magnitude in the *ASAS-3* catalog vs. the  $V$  magnitude. The significance of the numbers is discussed in Sec. 3.

equivalent widths but we found that the scatter in the relation between our  $(B-V)_0$  and the Balmer line equivalent widths given in Rodgers et al. (1993b) is much larger than for the relations with  $(V-J)_0$  and  $(J-K)_0$ . We therefore only used the relations with  $(V-J)_0$  and  $(J-K)_0$  (given above) to derive  $(B-V)$ . The scatter in these relations is shown in Fig. 1(b) and Fig. 1(c) and the difference between the  $(B-V)$  derived from the two relations is shown in Fig. 1(a). The  $(V-J)$  relation was not used for stars with  $V > 14.5$  because the  $V$  magnitude is poorly determined for fainter stars. For stars with  $V < 14.5$ , the color given in col. (3) of Table 1 is followed by a single colon and can be assumed to have an error of  $\sim 0.1$  magnitude. For stars with  $V > 14.5$ , the colors are followed by a double colon and can be assumed to have an error of  $\sim 0.2$  mag.. Only a few of these stars (75 (Pn241-13), 104 (Pn2312-58), 132 (Pn241-20) and 159 (Pn241-60)) have colors that may be blue enough for them to be possible BHB candidates.

The stars in Table 1 are given in order of RA and identified by a running number (col. 1) and the ID given by Rodgers et al. (1993a) (col. 2); the former is used throughout the rest of this paper. The coordinates of the brighter stars given by Rodgers et al. (1993a) were taken from the *HST* Guide Star Catalog and are accurate to one or two arcsec and are not repeated here. The coordinates of some of the fainter stars, however, were of lower accuracy and improved coordinates (taken from the USNO B Catalog) are given for them in Table 9 in the Appendix B.1.

### 3. THE VARIABILITY OF THE PROGRAM STARS IN THE *NR* FIELD.

Before discussing the colors of our program stars, we need to test them for variability. Fig. 2 (left) shows a plot of the scatter in the individual magnitudes ( $\Sigma_{mR}$ ) against their red magnitude ( $m_R$ ) as given in the Northern Sky Variability Survey (Woźniak et al. 2004). Most of these stars show a well-defined trend of increasing scatter with increasing  $m_R$ . Stars that show more scatter than this trend (at roughly more than the  $2\sigma$ -level) are shown by filled circles and labelled with the number of

TABLE 2  
STARS SHOWING EVIDENCE OF VARIABILITY.

No. <sup>a</sup>	ID <sup>b</sup>	RA	DEC	Spectral Type <sup>c</sup>	Period (days)	Type <sup>d</sup>	Notes
		J 2000					
12	CS 29521-078	23:10:43.0	+10:36:03	A0	...	EC?	(1)
16	IX PEG	23:11:12.9	+13:50:56	A2	0.601	RR $ab$	(2)
37	14601441	23:14:17.5	+02:37:31	A7	0.554	EC	(3)
47	11843625	23:15:46.0	+09:18:01	F0	0.381	EC	(4)
84	NSVS 11847482	23:21:51.0	+12:47:24	A3	0.555	RR $ab$	(5)
164	NSVS 14611789	23:32:18.8	+06:47:03	F0	...	...	(6)
168	CS 30333-0136	23:32:59.0	+08:26:14	A3	...	...	(7)
169	NSVS 9062655	23:33:14.7	+09:00:57	A1	...	...	(8)
173	NSVS 9063965	23:34:58.9	+13:44:06	F0	0.694	RR $ab$	(9)
A	NSVS 9062108	23:31:50.0	+12:51:00	...	0.328	EC	(10)

<sup>a</sup> Number given in Table 1 and Fig. 2. A is described in text.

<sup>b</sup> Identification

<sup>c</sup> Rodgers et al. (1993b)

<sup>d</sup> RR = RR Lyrae; EC = Contact binary.

(1) Norris et al. (1999) give  $V = 13.65$ ,  $(B - V) = +0.34$ ,  $(U - B) = +0.01$  in their search for stars of low metal abundance but this star is not included in the Beers et al. (2000) catalog of metal-weak stars. We found  $V = 13.58$ ,  $(B - V) = 0.334$  and  $(u - B)_K = +1.730$ ; this suggests that the star is probably a low-amplitude contact binary.

(2) Wils et al. (2006) and Kinemuchi et al. (2006) give periods of 0.60099 and 0.60103 days respectively. Both periods are based on *NSVS* data. Our photometric and spectroscopic observations are discussed in Sec. 4.

(3) The period is from the catalog of Gettel et al. (2006) who list it as a contact binary with a  $V$  amplitude of 0.393 mag.

(4) The period is from the catalog of Gettel et al. (2006) who list it as a contact binary with a  $V$  amplitude of 0.325 mag.

(5) Wils et al. (2006) and Kinemuchi et al. (2006) give periods of 0.55515 and 0.55514 days respectively. Both periods are based on *NSVS* data. Our photometric and spectroscopic observations are discussed in Sec. 4.

(6) The evidence for variability from the *NSVS* data is not supported by that from the *ASAS-3* catalog (Pojmański, 2002).

(7) The evidence for variability from the *NSVS* data is not supported by that from the *ASAS-3* catalog. The catalog of HB and metal-weak stars (Beers et al. 2007a) gives  $V = 12.18$ ,  $(B - V) = 0.23$  and  $(U - B) = +0.17$  compared with our  $V = 12.20$ ,  $(B - V) = +0.234$  and  $(u - B)_K = 2.034$ . We classify it as a BHB star.

(8) The evidence for variability from the *NSVS* data is not supported by that from the *ASAS-3* catalog. We classify it as a BHB star.

(9) Wils et al. (2006) and Kinemuchi et al. (2006) give periods of 0.69425 and 0.69417 days respectively. Both periods are based on *NSVS* data. Our photometric and spectroscopic observations are discussed in Sec. 4.

(10) The period is taken from the *ASAS-3* catalog where the star is classified as RRc/EC. The 2MASS colors  $(J - K)_0 = 0.23$  and  $(V - J)_0 \sim 1.0$  are too red, however, for it to be an RRc. Spectra taken on 2009 Dec 19 UT with the FAST spectrograph of the Whipple Observatory 1.5-m telescope (spectral resolution 2.3 Å;  $S/N = 30$ ) show that this star and the eclipsing star No. 37 had a FWHM for the  $\lambda 4481$  line of 2.4 and 2.6 Å respectively. These FWHM are substantially larger than the FWHM of 1.1 and 1.2 Å found for the RR Lyrae stars Nos. 16 and 18 respectively from spectra taken on the same night. This line width difference strongly supports the classification of this star as an eclipsing binary (Kinman & Brown, 2010).

the star (Table 1, col. 1). Fig. 2 (right) shows a similar plot of the error of a single observation in  $V$  of a star in the *ASAS-3* catalog (Pojmański, 2002) against its  $V$  magnitude. The numbered stars in Fig. 2 (left) are also shown by numbered filled circles in Fig. 2 (right). The star marked A in both plots is NSVS 9062108 (23:31:50, +12:51:00 (2000)); it is listed in the *ASAS-3* catalog as type RRC/EC with  $12.05 < V < 12.43$  and a period of 0.328712 days. More information about these stars (including previous identifications as variables) is given in the notes to Table 2. In summary, three (16, 84 and 173) are RR $ab$  stars, four (12, 37, 47 and A) are eclipsing stars and the remaining three (164, 168 and 169) are probably not variable. We have made new photometric and spectroscopic observations of the three RR Lyrae stars and these are discussed in Sec. 4.

The RR Lyrae star IO PEG (period = 0.567 days;  $15.0 < m_{pg} < 16.5$ ; Goranskij, 1986) is too faint to be listed in the *NSVS* and has only 3 observations in the *ASAS-3* catalog ( $\langle V \rangle = 15.3 \pm 0.3$ ). Although its magnitude is uncertain, we take it to be fainter than the limit of the *NR* survey.

#### 4. RR LYRAE STARS.

##### 4.1. RR Lyrae stars in NR

In addition to BHB stars, RR Lyrae stars are important tracers of the halo. In our discussion of the variability of the stars in the *NR* field in Sec. 3, we found that Nos 16, 84 and 173 (Table 2 and Fig. 2) are type  $ab$  RR Lyrae stars. We made photometric observations of these stars in 2008 and 2009 with the commercial robotic f/7 0.8-m telescope of the Tenagra Observatory in Arizona which has a 1024×1024 SITe CCD. Details of similar photometry with this telescope are given by Kinman & Brown (2010). Periods were determined from this data using the periodogram program of Horne & Baliunas (1986). The period of 0.601089 days found for No. 16 (IX Peg) is satisfactorily close to the periods of 0.60103 days and 0.60099 days that were found by Kinemuchi et al. (2006) and Wils et al. (2006) respectively from the Northern Sky Variability Survey (*NSVS*) data (Wóznia et al. 2004). The periods of 0.555135 and 0.6945125 days found for Nos 84 and 173 respectively are also close to the periods of 0.55514 and 0.69417 days that Kinemuchi et al. (2006) found for them. The light curves for these

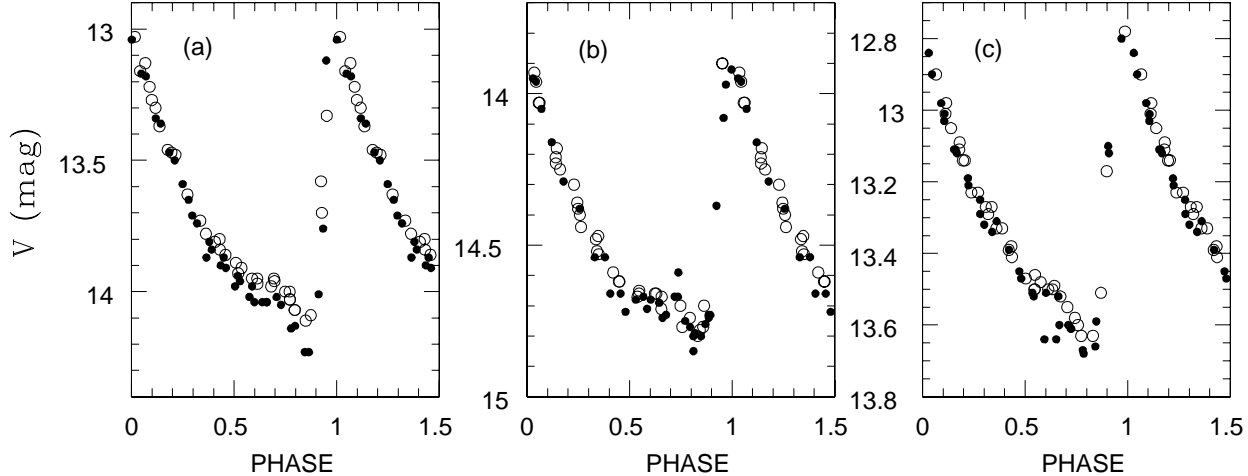


FIG. 3.—  $V$ -magnitude light curves for three type *ab* RR Lyrae stars in the *NR* field; (a) No. 16 (Pn2312-1); (b) No. 84 (Pn2312-38) and (c) No. 173 (Pn2312-41). Filled circles are Tenagra observations in 2008 and open circles are Tenagra observations in 2009.

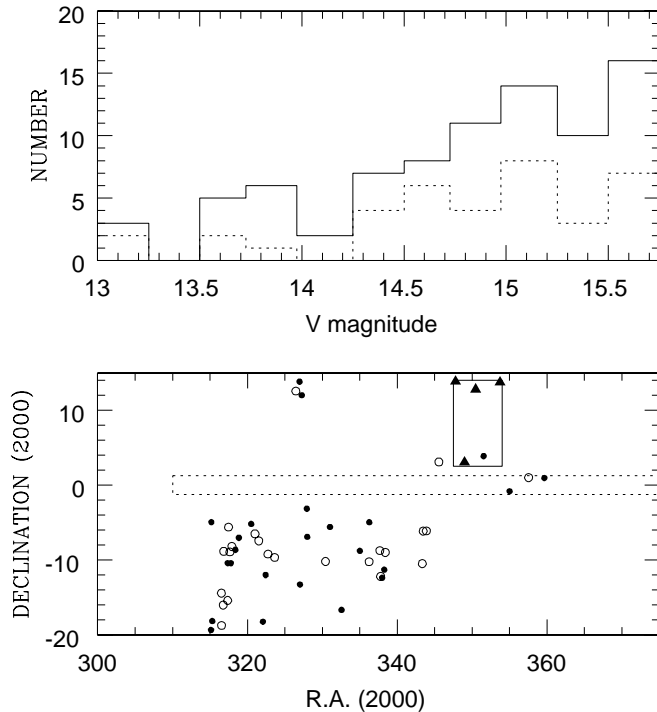


FIG. 4.— (above) The number of RR Lyrae stars per 0.25 mag. interval in 400 deg<sup>2</sup> of the *LONEOS* survey near the *NR* field. The full histogram shows the total number and the dotted histogram those with a  $V$ -amplitude less than 0.75 mag. (below) The location of the stars in the *LONEOS* survey. Those with  $V < 14.75$  are shown by filled circles and those with  $14.75 \leq V \leq 15.25$  by open circles. The four *NSVS* stars in the *NR* field are shown by filled triangles. The location of the *NR* field is shown by the solid rectangle and the *SDSS* Stripe 82 field is shown by the dotted rectangle.

stars are given in Fig. 3. Metallicities  $[\text{Fe}/\text{H}]$  were derived from the amplitudes and periods (using eqn. 6 in Sandage (2004)) and are given with other photometric data in Table 3.

Radial velocities were measured from spectra taken in December 2009 with the FAST spectrograph of the Whipple 1.5-m telescope (resolution 2.3 Å and waveband  $\lambda\lambda$  3600–5500 Å). The  $\gamma$ -velocities were derived following Liu (1992). The spectra of Nos 16 and 84 were

were taken close to maximum light and so were not suitable for deriving  $[\text{Fe}/\text{H}]$  from the Ca II K-line equivalent width. The spectrum of No. 173 was taken at phase 0.451, however, so we were able to derive an  $[\text{Fe}/\text{H}]$  of  $-1.99$  by the  $\Delta S$ -method (Preston 1959). This  $[\text{Fe}/\text{H}]$  is in satisfactory agreement with the  $-2.15$  derived from the amplitude and period. The spectroscopic data for these stars are summarized in Table 3.

Kinemuchi et al. (2006) found a fourth and fainter type *ab* RR Lyrae star (*NSVS* 14602495; R.A. 23:15:56.66, DEC. +03:02:58 (2000)) within the *NR* field but not identified by Rodgers et al. (1993a). It has a period of 0.59355 days and a  $V$  amplitude of 1.56 mag, from which they derived an  $[\text{Fe}/\text{H}]$  of  $-2.60$ . Our  $V$  amplitudes are less than theirs by a factor of  $0.70 \pm 0.06$ , so the amplitude of this star is 1.09 mag. on our scale. This implies an  $[\text{Fe}/\text{H}]$  of  $-1.9$  according to Sandage (2004). Kinemuchi et al. also give an intensity-weighted  $V$ -magnitude of 15.03 mag. Their mean  $V$ -magnitudes are calculated from *NSVS* unfiltered CCD magnitudes and (for the other three RR Lyrae stars) average 0.26 mag fainter than the intensity-weighted  $V$  magnitudes that we derived from our photometry. We have therefore assumed an intensity-weighted  $V$ -magnitude of 14.77 for this star and an absolute  $V$  magnitude of  $+0.45$  (following Clementini et al. (2003)) to derive a distance of 6.67 kpc.

#### 4.2. RR Lyrae stars in LONEOS Survey

The *LONEOS* survey for RR Lyrae stars by Miceli et al. (2008) covers the sky in the neighborhood of the *NR* field; they discovered 838 type *ab* RR Lyrae stars in this field. Fig. 4 (below) shows the location of the stars in this survey that have  $V < 15.25$  and that have  $21^h < \text{R.A.} < 01^h$  and declinations between  $-20^\circ$  and  $+15^\circ$ ; the  $V$  magnitude distribution of the brighter of the *LONEOS* variables is shown in Fig. 4 (above). About 45% of this sample have  $V$  amplitudes of less than 0.75 mag. One of these lower amplitude variables lies in the *NR* field but is not identifiable as a variable in the *NSVS* because it lies close to a brighter star.

The sample of *LONEOS* stars shown in Fig. 4 cover roughly 400 deg<sup>2</sup> and contains 31 stars with  $V \leq 14.75$  and 42 stars with  $V \leq 15.00$ . We might therefore expect

TABLE 3  
DATA FOR THREE RR LYRAE STARS IN THE *NR* FIELD.

ID <sup>a</sup>	Star 16	Star 84	Star 173
<i>GCVS</i>	IX PEG	...	...
<i>NSVS</i>	11840238	11847482	9063965
RA(J2000)	23:11:12.84	23:21:50.95	23:34:58.88
DEC(J2000)	+13:50:56.2	+12:47:24.5	+13:44:06.3
Type	<i>ab</i>	<i>ab</i>	<i>ab</i>
Period (days)	0.601089	0.555135	0.694125
JD(max) <sup>b</sup>	2454776.9770	2451444.6900	2454777.5497
$\langle V \rangle^c$	13.676	14.443	13.269
$V_{max}$	13.030	13.900	12.780
$V_{min}$	14.158	14.801	13.655
Rise Time	0.160	0.175	0.220
$\phi_{31}$	2.05	1.82	2.42
$E(B - V)$	0.070	0.059	0.071
$[Fe/H]^d$	-2.02	-1.41	-2.15
$[Fe/H]^e$	-2.43	...	-2.16
JD(hel) <sup>f</sup>	2455184.5558	2455184.6159	2455184.6201
T <sup>g</sup>	300	270	270
Phase <sup>h</sup>	0.067	0.966	0.451
Rad. Vel. <sup>i</sup>	$-359.8 \pm 5.1$	$-113.8 \pm 4.6$	$-098.6 \pm 5.9$
Rad. Vel. <sup>j</sup>	-325.9	-87.5	-104.4
$\Delta S^k$	...	...	10.0
$[Fe/H]^l$	...	...	-1.99
$M_v^m$	0.428	0.558	0.434
Distance <sup>n</sup>	4.01	5.47	3.31

<sup>a</sup> No. of star in Table 1.

<sup>b</sup> Heliocentric Julian Date of maximum light.

<sup>c</sup> Intensity-weighted mean  $V$  magnitude.

<sup>d</sup> Derived from eqn. (6) in Sandage (2004).

<sup>e</sup> Kinemuchi et al. (2006).

<sup>f</sup> Heliocentric Julian Date of mid-exposure of spectrum.

<sup>g</sup> Integration time for spectrum in seconds.

<sup>h</sup> Phase of spectrum.

<sup>i</sup> Observed radial velocity in  $\text{km s}^{-1}$  relative to LSR.

<sup>j</sup>  $\gamma$ -velocity in  $\text{km s}^{-1}$  relative to LSR.

<sup>k</sup> Preston (1959)  $\Delta S$  derived from the calibration of equivalent widths given in Kinman & Carretta (1992).

<sup>l</sup> Derived from  $\Delta S$  following Suntzeff et al. (1994).

<sup>m</sup> Absolute  $V$  magnitude from  $[Fe/H]$  following Clementini et al. (2003).

<sup>n</sup> Distance in kpc.

5 and 7 stars in these magnitude intervals, respectively, in the  $70^\circ$  of *NR*.

## 5. THE RADIAL VELOCITY DISTRIBUTION IN THE *SR* FIELD.

We begin by discussing the radial velocity distribution of stars in the *SR* field. The *SR* field covers a pair of overlapping *SERC UKSTU* objective prism fields with plate centers at  $03^h 40^m$ ,  $-65.^\circ 0$  and  $03^h 48^m$ ,  $-60.^\circ 0$ . Rodgers et al. (1993a) list 259 early-type stars in this field and give radial velocities for 191 of them. This field has the same galactic coordinates as the  $(l, b) = (270^\circ, -45^\circ)$  field observed by Gilmore et al. (2002) although the *SR* field covers a much larger area to a brighter limiting magnitude. Fig. 5 shows the distributions of the heliocentric radial velocities of both the *SR* (above) and *NR* fields; in both cases these histograms refer to early-type stars that are brighter than  $V = \sim 15$ . The red histogram in the upper figure shows the distribution of the stars with  $V \leq 18$  given by Gilmore et al. (2002); the numbers of these turn-off stars have been normalized to be the same as for the early-type stars in the *SR* field. At this galactic latitude ( $b = -45^\circ$ ), the heliocentric velocity will be about 70% of the galactic rotational velocity. Gilmore et al. describe the velocity distribution

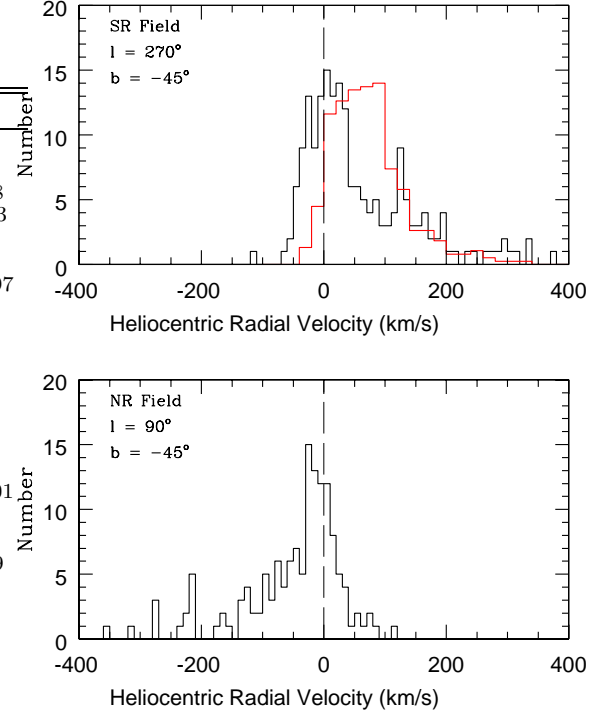


FIG. 5.— Distribution of the heliocentric radial velocities ( $V_{hel}$ ) in  $\text{km s}^{-1}$  for the *SR* (above) and *NR* (below) fields are shown by the black histograms for the early-type stars found by Rodgers et al. (1993). The red histogram shows the distribution of the turn-off stars found in the  $(l, b) = (270^\circ, -45^\circ)$  field with  $V < 18$  by Gilmore et al. (2002). The total number of the turn-off stars has been normalized to equal that of the early-type stars.

for their  $V < 18$  stars as that to be expected for a canonical thick-disk with a lag of less than  $50 \text{ km s}^{-1}$ . Their velocity distribution (the red histogram) actually shows a broad peak between 0 and  $+100 \text{ km s}^{-1}$ , and so the lag seems more like  $70 \text{ km s}^{-1}$  but this is a minor point. The velocity distribution for the early-type stars in the *SR* field, on the other hand, shows a broad asymmetrical peak centered on  $+5 \text{ km s}^{-1}$  that continues out to large positive velocities (like the red histogram).

The radial velocity distribution of the early-type stars differs quite markedly from that of the turn-off stars: the distribution for the early type stars has a peak that is close to zero, and so the early type stars presumably have a significant old thin disk component (which according to Gilmore et al. should have a lag of  $\sim 20 \text{ km s}^{-1}$ ). “Early-type stars,” however, comprise a wide variety of types with a range of scale-heights (Preston et al. 1994; Knude 1997) and so it is probably over-simplistic to characterize them as belonging to either thin disk, thick disk or halo as may be done for turn-off stars.

The early-type stars in the *SR* field also show a peak in their heliocentric radial velocities at  $+125 \text{ km s}^{-1}$ ; this corresponds to a lag of  $+180 \text{ km s}^{-1}$  which is what one might expect for a prograde halo. Both the early-type stars and the turn-off stars show extended distributions of heliocentric radial velocities to  $+350$  to  $+400 \text{ km s}^{-1}$  which shows that both contain a significant component of halo stars with retrograde orbits; Gilmore et al. (2002) already noted this for their turn-off stars that have  $V > 18$ .

Too great a correspondence between different *tracer*

TABLE 4  
COMPARISON OF  $NR$  RADIAL VELOCITIES WITH THOSE FROM OTHER SOURCES.

No.	ID <sup>a</sup>	$NR_{LSR}$ <sup>b</sup> km s <sup>-1</sup>	$NR_{helio}$ <sup>c</sup> km s <sup>-1</sup>	$RV_{KPNO}$ <sup>d</sup> km s <sup>-1</sup>	$RV_{Century}$ <sup>e</sup> km s <sup>-1</sup>	$RV_{Adopted}$ <sup>f</sup> km s <sup>-1</sup>
4	Pn241-37	+015	+009	+019	...	+013
16	Pn2312-1	-352	-358	-351	...	-355
38	Pn241-51	-147	-153	-186	...	-171
41	Pn2312-14	-256	-262	-289	...	-277
48	Pn241-45	-130	-136	-104	...	-121
60	Pn241-42	-207	-213	-216	...	-216
63	Pn2312-2	-018	-024	...	-065	-045
72	Pn2312-4	+014	+008	...	-002	+002
90	Pn2312-36	-025	-031	...	-020	-028
99	Pn2312-22	-201	-207	-232	-217	-221
110	Pn2312-28	-061	-067	...	-0054	-062
115	Pn241-55	-142	-148	-127	...	-140
120	Pn241-56	-047	-053	-086	...	-072
126	Pn2311-18	...	...	...	-057	-059
128	Pn2312-30	+063	+057	+047	...	+050
134	Pn241-8	-117	-123	-140	...	-134
140	Pn2312-53	-038	-044	...	-051	-050
141	Pn241-22	-116	-122	-123	...	-125
145	Pn241-4	-131	-137	-174	...	-158
146	Pn241-27	-038	-044	-066	...	-057
148	Pn241-26	-070	-076	...	-027	-054
151	Pn241-6	+043	+037	+045	...	+039
157	Pn2311-39	-056	-062	-051	-0052	-057
158	Pn241-28	+042	+036	+033	...	+032
163	Pn2312-43	+015	+009	...	000	+002
169	Pn2312-45	000	-006	-030	...	-020

<sup>a</sup> ID from Rodgers et al. (1993b)

<sup>b</sup> Radial velocity relative to LSR. Rodgers et al. (1993b)

<sup>c</sup> Heliocentric radial velocity. Rodgers et al. (1993b)

<sup>d</sup> Heliocentric radial velocity. (This paper).

<sup>e</sup> Heliocentric radial velocity. (Brown et al. 2008).

<sup>f</sup> Adopted radial velocity relative to LSR.

populations should not be expected. Stars as closely related as RR Lyrae stars and BHB stars can show different kinematics in the same field (Kinman et al. 2007a), and the ratio of BHB to turn-off stars can vary (Bell et al. 2010). Nevertheless, further observations of the early-type stars in the  $SR$  field would be of interest; in particular, an investigation of the sharp peak in their radial velocities at  $\sim +125$  km s<sup>-1</sup>. A list of these stars and a brief discussion of their possible nature is given in Appendix A.

## 6. THE METALLICITIES AND RADIAL VELOCITIES OF THE PROGRAM STARS IN THE $NR$ FIELD.

### 6.1. *Metallicities.*

We now consider the metallicities of the early-type stars in the  $NR$  field. In their second paper, Rodgers et al. (1993b) give the equivalent widths of the Ca II K line and the H $\delta$  Balmer line for 141 of their program stars. They do not derive metallicities for the individual stars but, in their third paper, Rodgers et al. (1993c) used these equivalent widths to show that many of their program stars have  $[\text{Fe}/\text{H}] < -1.0$ . They conclude that while some of these metal-poor stars have halo kinematics, a significant proportion of those with  $V < 14$  (which they took to be less than 2.5 kpc above the plane) have kinematics that are consistent with them belonging to a metal-weak thick disk.

We derive a metallicity  $[\text{m}/\text{H}]$  for each star from a plot of the equivalent width of its Ca II K line against

$(B - V)_0$  using the calibration given in Fig. 9 of Clewley et al. (2002). These metallicities and the data from which they are derived are given in Table 11 in Appendix B. The equivalent width  $W_0(K)$  of the Ca II K line given by Rodgers et al. (1993b) was corrected for an interstellar component  $W(K)$  of 0.6 Å. The value of  $W(K)$  is discussed in Appendix D where we conclude that a value of 0.3 Å would be more appropriate than the 0.6 Å correction used by Rogers et al. (1993b). We therefore also computed metallicities for the program stars using  $W(K) = 0.3$  Å and these are given in the last column of Table 11 in Appendix B. Our derived metallicities  $[\text{m}/\text{H}]$  can only be considered approximate because of the combined errors of  $W(K)$  and  $(B - V)_0$  and the uncertainties in the calibration plot. This will be particularly the case for the hottest and most metal-poor stars where the K-line is weak and also for the faintest stars for which the measured equivalent widths are likely to be the least accurate. Brown et al. (2008) give  $[\text{Fe}/\text{H}]$  for six of these stars. The mean difference of the  $[\text{m}/\text{H}]$  in the last column of Table 11 and the  $[\text{Fe}/\text{H}]$  of Brown et al. (2008) for these stars is  $+0.35 \pm 0.27$ . We therefore consider that although these  $[\text{m}/\text{H}]$  have statistical value, their individual values should be taken with considerable reserve.

### 6.2. *Radial Velocities of program stars in the $NR$ Field.*

We now discuss the radial velocities that are available for the early-type stars in the  $NR$  field. Rodgers et al. (1993b) give radial velocities for their program stars



that were obtained with the coude spectrograph of the Mt Stromlo 1.88-m telescope. The detector was the Mt Stromlo Photon Counting Array which gave a resolution of  $2.4 \text{ \AA}$  over the waveband  $\lambda\lambda 3830$  to  $4370 \text{ \AA}$ . The velocities were given with respect to the local standard of rest (LSR) by adding  $+6.0 \text{ km s}^{-1}$  to the heliocentric velocities; their probable error was estimated to be  $18 \text{ km s}^{-1}$ . Spectra of 18 of these program stars were obtained with RC spectrograph of the Mayall 4-m telescope at Kitt Peak; the spectral resolution was  $0.8 \text{ \AA}$  over the waveband  $\lambda\lambda 3880$  to  $4580 \text{ \AA}$  (for further details see Kinman et al. 1996). The heliocentric radial velocities from these spectra were kindly supplied by Dr Nick Suntzeff (priv. comm. 1996, 1998); their estimated errors are  $\sim 5 \text{ km s}^{-1}$ . Radial velocities of 8 of the program stars are available from the *Century Survey* (Brown et al. 2008). These spectra were taken with the FAST spectrograph on the Whipple 1.5-m telescope (resolution  $2.3 \text{ \AA}$ , waveband  $\lambda\lambda 3450$  to  $5450$ ,  $S/N = 30$ ). These velocities have an estimated error of  $16 \text{ km s}^{-1}$ .

These velocities are compared in Table 4. The mean difference of Stromlo *minus* Kitt Peak is  $+8.1 \pm 4.9 \text{ km s}^{-1}$  where the *rms* of a single difference is  $20.3 \text{ km s}^{-1}$ . The mean difference of Stromlo *minus* Whipple is  $-0.7 \pm 8.7 \text{ km s}^{-1}$  and the *rms* of a single difference is  $24.5 \text{ km s}^{-1}$ . These differences are in satisfactory agreement with quoted errors from the individual sources and there is no evidence for any systematic error in the Stromlo velocities. The adopted radial velocities with respect to the LSR are given in the final column of Table 3. Our corrections to the LSR have been made separately for each star and *not*, as was done by Rodgers et al. (1993b), with a single correction for the whole field.

## 7. THE SELECTION OF THE BLUE HORIZONTAL BRANCH (BHB) STARS IN THE *NR* FIELD.

The blue horizontal branch of a globular cluster can be quite complex (e.g. as in NGC 2808 (Dalessandro et al. 2010)) and here we consider only those BHB stars with effective temperatures ( $T_{eff}$ ) less than  $\sim 10,000 \text{ K}$  (called HBA stars by Möhler (2004)). The primary criterion for selecting *field* BHB stars is that they lie close to the Zero Age Horizontal branch (ZAHB) in a plot of  $\log T_{eff}$  vs  $\log g$  (see Fig. 5 in Behr (2003)). Fig. 6 shows a plot of  $T_{eff}$  vs.  $(B - V)_0$  for 25 local BHB stars;  $T_{eff}$  is taken from Kinman et al. (2000) (black circles), Behr (2003) (green circles) and For and Sneden (2010) (red circles) and the  $(B - V)_0$  is taken from Kinman et al. (2000). This shows that the errors are substantial even when high-resolution ( $> 15,000$ ) and high  $S/N$  spectra are available and these limit our ability to distinguish BHB stars from other types — especially for  $T_{eff} \geq 10,000 \text{ K}$  where the ZAHB and Main Sequence converge in the  $T_{eff}$  vs  $\log g$  plot. In this paper we use colors as surrogates for  $\log g$  and  $\log T_{eff}$  and calibrate these color-color plots using local bright BHB stars that have been identified by the authors referred to above.

Preston et al. (1991) identified BHB stars by their position in a plot of the gravity-sensitive  $(U - B)_0$  index against  $(B - V)_0$  over the range  $-0.02 \leq (B - V)_0 \leq 0.18$ . This is an appropriate range of  $(B - V)_0$  since the blue end roughly corresponds to  $T_{eff} = 10,000 \text{ K}$  and the red end corresponds to the blue edge of the instability gap

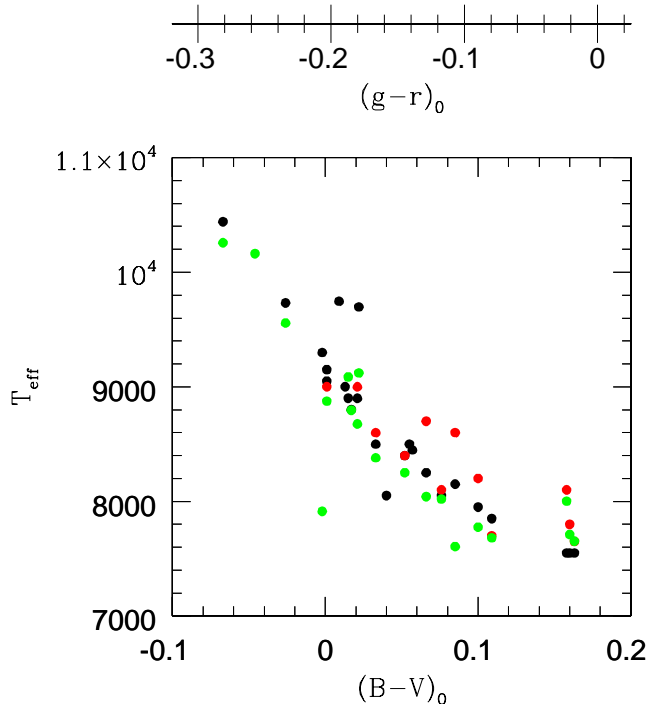


FIG. 6.—  $T_{eff}$  (ordinate) vs.  $(B - V)_0$  for 25 local BHB stars. The  $T_{eff}$  are taken from Kinman et al. (2000) (black circles), Behr (2003) (green circles) and For & Sneden (2010) (red circles). All  $(B - V)_0$  are taken from Kinman et al. (2000). The  $(g - r)_0$  scale is approximate.

Sandage (1990). The Strömgren  $u$  filter is better than the Johnson  $U$  filter for use with the Johnson  $B$  filter for measuring the Balmer jump. Consequently, in this paper we use the  $(u - B)_{K0}$  index as defined by Kinman et al. (1994) as our primary discriminant. This index was measured for 67 stars in the *NR* field. These include all those stars in the appropriate  $(B - V)_0$  range with  $V_0 \leq 15.0$  except for stars 97, 104, 122, 126, 139, 148 and 162. For these latter stars we used the  $(NUV - V)_0$  index as a discriminant as described by Kinman et al. (2007b).

### 7.1. Selection using the $(B - V)_0$ vs. $(u - B)_{K0}$ Plot.

The  $(B - V)_0$  vs.  $(u - B)_{K0}$  plot is shown in Fig. 7. Here, nearby BHB stars whose classification is secure (Kinman et al. 2000; Behr 2003) are shown as filled triangles that lie on a well-defined curve. The dotted lines in Fig. 7 enclose an area in which  $(B - V)_0 \leq 0.18$  and  $(u - B)_{K0}$  is within  $\pm 0.075 \text{ mag.}$  of the curve defined by the nearby BHB stars. Stars that lie within this area are shown as red filled circles while those whose error bars lie within or very close to this area are shown as green filled circles. Error bars are also shown for the five stars (3, 27, 106, 121, & 136) for which there is some evidence that they might be BHB stars.

### 7.2. Selection using the $(B - V)_0$ vs. $(NUV - V)_0$ plot.

The  $(B - V)_0$  vs.  $(NUV - V)_0$  plot is shown in Fig. 8. The dotted parallelogram (taken from Kinman et al. 2007b) shows the expected location of the BHB stars. The red and green filled circles show the stars that are in or close to the BHB location in Fig. 7; these stars also lie satisfactorily close to the defining area in Fig. 8. There are, however, three stars (121, 136 & 162) that



TABLE 5  
BHB CANDIDATES AMONG EARLY-TYPE STARS IN *NR*

No.	$V_0$	$(B - V)_0$ <sup>a</sup>	$P_{u-B}$ <sup>b</sup>	$P_{NUV}$ <sup>c</sup>	$P_\beta$ <sup>d</sup>	$P_{CHSS}$ <sup>e</sup>	$P_{B2M}$ <sup>f</sup>	[m/H] <sup>g</sup>	RV <sup>h</sup> km s <sup>-1</sup>	Class <sup>i</sup>
2	12.15	+0.198	-3	0	-3	...	...	-0.8	+000	BHB1
3	13.15	-0.031	-3	...	...	...	H	-2.0	-218	BHB1
4	13.07	+0.144	+4	+4	-3	...	...	-1.2	+013	BHB2
15	14.87	+0.038†	+2	+4	...	...	...	>0.0	-211	BHB3
17	12.33	+0.180	-3	+2	...	...	...	-0.8	-007	BHB1
27	12.62	+0.164	-3	0	...	...	...	-1.5	+071	BHB1
30	14.53	-0.049	+4	+4	...	...	...	-2.0	-227	BHB3
34	13.14	+0.237	-3	-3	...	...	H	-0.3	-004	BHB1
38	12.75	+0.045	+4	+4	+3	...	...	-2.2	-171	BHB3
41	14.29	+0.023†	+4	+4	...	...	H	-2.2	-277	BHB3
48	14.43	+0.020†	+2	...	...	...	H	-0.8	-121	BHB1
52	14.06	+0.246	-3	-3	...	...	H	-0.7	-161	BHB1
53	13.62	+0.122	+2	+4	...	...	...	-1.4	-029	BHB3
56	13.50	-0.261†	...	...	...	...	H	...	...	BHB1
60	14.62	+0.057	+2	+2	...	...	H	-2.6	-216	BHB2
63	14.60	+0.184	0	...	...	0	...	<b>-1.13</b>	-045	BHB1
72	14.84	+0.282	-3	-3	...	0	...	<b>-0.94</b>	+002	BHB1
77	11.93	+0.158	+2	+2	-3	...	H	-0.9	-007	BHB1
79	13.58	-0.062†	0	-3	...	...	H	-2.0	+006	BHB1
83	14.63	+0.090	-4	-3	...	...	H	-1.2	-114	BHB1
87	15.2	+0.53†	...	-3	...	...	H	...	-281	BHB1
90	12.80	-0.063	0	-3	...	-4	...	<b>0.00</b>	-028	BHB1
92	15.53	+0.037	+2	+2	...	...	...	-1.0	-228	BHB2
94	13.6	+0.4	...	-3	...	...	H	...	-073	BHB1
99	14.53	+0.104	+4	+4	...	+4	...	<b>-2.14</b>	-221	BHB3
104	15.1	+0.150	...	+2	...	...	H	-2.7	-273	BHB1
106	12.44	+0.132	-3	-3	...	...	H	+0.0	+070	BHB1
110	14.91	+0.073	+4	+4	...	+4	...	<b>-3.00</b>	-062	BHB3
115	14.37	+0.042	+4	+4	...	...	...	-1.8	-140	BHB3
116	12.89	+0.195	-3	0	...	...	H	-1.3	-017	BHB1
120	12.88	+0.198	0	0	+3	...	...	-1.6	-072	BHB2
121	14.59	+0.124	-3	+4	...	...	...	-1.4	-027	BHB1
122	14.2	+0.18†	...	...	...	...	M	...	...	BHB1
126	14.1	-0.1	...	-3	...	-4	...	...	<b>-059</b>	BHB1
128	12.22	+0.057	+4	+4	+3	...	H	-1.8	+050	BHB3
133	14.84	+0.176	+2	0	...	...	...	-1.8	-009	BHB1
134	13.96	+0.148	+2	+4	...	...	...	-0.4	-134	BHB3
136	11.05	+0.074	-3	+4	-3	...	H	-1.6	+023	BHB1
138	10.78	+0.097	-3	...	-3	...	...	-1.2	-017	BHB1
140	13.70	+0.265	...	-3	...	-4	H	<b>-1.04</b>	-050	BHB1
141	14.08	+0.208	+2	-3	...	...	...	-1.5	-125	BHB1
143	11.89	+0.116	-3	-3	-3	...	H	-1.4	+009	BHB1
145	12.64	+0.027	+4	+4	-3	...	...	-0.2	-158	BHB2
146	13.46	+0.058	+4	+4	...	...	H	+0.0	-057	BHB3
148	14.20	+0.089	...	0	...	0	H	<b>-0.25</b>	-054	BHB1
151	14.64	+0.009	+4	+4	...	...	...	>0.0	+039	BHB3
156	13.73	+0.299	...	-3	-3	...	M	-1.9	-106	BHB1
157	12.81	+0.073	+4	+4	+4	+4	H	<b>-0.75</b>	-057	BHB3
158	12.47	+0.165	+4	+4	-3	...	...	+0.0	+032	BHB2
161	12.63	+0.261	...	-3	...	...	H	-1.3	-044	BHB1
162	13.99	+0.062†	...	+4	...	...	H	-2.3	-025	BHB2
163	14.37	+0.227	...	-3	...	0	H	<b>-0.91</b>	+002	BHB1
168	11.96	+0.158	-3	+2	-3	...	H	-0.6	+020	BHB1
169	13.83	+0.047	+4	+4	...	...	M	-2.0	-020	BHB3

<sup>a</sup> † Outside defining window in  $(J - H)_0$  vs.  $(H - K)_0$  plot. See Fig. 10(c) and Fig. 10(d).

<sup>b</sup> BHB class from  $(u - B)_{K0}$  vs.  $(B - V)_0$  plot. See Sec. 7.5.

<sup>c</sup> BHB class from  $(V - NUV)_0$  vs.  $(B - V)_0$  plot. See Sec. 7.5.

<sup>d</sup> BHB class from Strömgren  $\beta$  vs.  $(B - V)_0$  plot. See Sec. 7.5.

<sup>e</sup> BHB class in *Century* Survey, See Sec. 7.5.

<sup>f</sup> BHB class in B2M Survey; See Sec. 7.5.

<sup>g</sup> Metallicity from Ca II K line assuming correction for interstellar component of 0.3 Å (Rodgers et al. 1993b). Metallicities in bold-face are from Brown et al. (2008).

<sup>h</sup> Adopted radial velocity corrected to LSR. The velocity in bold-face is from Brown et al. (2008).

<sup>i</sup> Adopted Class. BHB3 are the most likely to be BHB stars and BHB1 are the least likely.

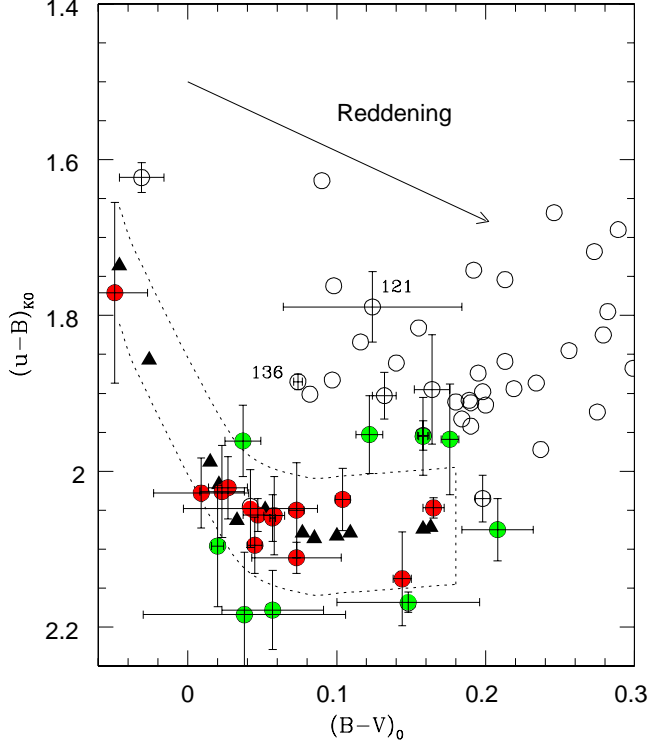


FIG. 7.— The ordinate  $(u-B)_{K0}$  is defined in Kinman et al. (1994). The abscissa is Johnson  $(B-V)_0$ . The data for the local BHB stars (filled triangles) are taken from Kinman et al. (2000). The location of these local BHB stars is used to define the window shown by dotted lines. The BHB star candidates are shown by red filled circles if they lie within this window and by green filled circles if their error bars lie within the window. The other program stars are shown by open circles.

are BHB stars according to their  $(NUV-V)_0$  index although stars 121 and 136 are not BHB stars according to their  $(u-B)_{K0}$  index. The  $NUV$  magnitude of star 136 is close to the saturation limit for this *GALEX* magnitude (Morrissey et al. 2007) so its  $NUV$  error may have been underestimated. Its identification as a BHB star is therefore uncertain.

### 7.3. Selection using the Strömgren $\beta$ vs. $(B-V)_0$ Plot.

The Balmer lines of BHB stars are narrower than those of higher-gravity main sequence stars of the same effective temperature and this property has been used to identify BHB stars (Searle & Rodgers, 1966; Pier, 1983). The Strömgren  $\beta$  index can be used as a surrogate for the commonly used  $D_{0.2}$  width as shown in the Strömgren  $\beta$  vs.  $(B-V)_0$  plot (Fig. 9b) in which the nearby BHB stars (filled circles) with  $+0.03 \leq (B-V)_0 \leq +0.18$  have a different location from the non-BHB stars. The data for the non-BHB stars in Fig 9(b) were taken from Crawford et al. (1972) (crosses), Gray & Garrison (1989) (open triangles) and Stetson (1991) (inverted filled triangles) while those for the nearby BHB stars were taken from Kinman et al. (2000). Fig. 9(a) shows the same plot for the brighter of our program stars for which  $\beta$  could be measured accurately enough with a 0.9-m telescope. We use the same symbols as in Fig. 7. Four of this sample (nos. 38, 120, 128 & 157) lie on the line that defines the BHB stars — supporting this classification for them. Five (nos. 4, 77, 145, 158 and 168) lie well above the BHB line. This casts doubt on their classification as BHB stars

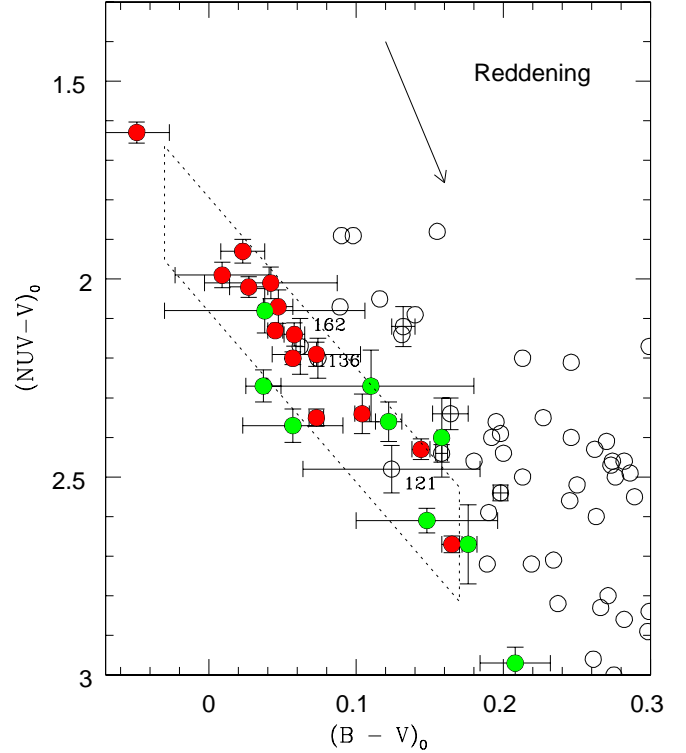


FIG. 8.— The ordinate is the de-reddened difference between the *GALEX*  $NUV$  magnitude (effective wavelength 2267Å) and the Johnson  $V$  magnitude. The abscissa is the Johnson  $(B-V)_0$  color. The dotted parallelogram is the expected location of the BHB star candidates (Kinman et al. 2007b). The symbols have the same meaning as in (Fig 7) and refer to their location in the  $(u-B)_{K0}$  vs.  $(B-V)_0$  plot (Fig. 7).

and we discuss this further in Sec. 8.2. Star 136, whose classification as a BHB star depends upon a questionable  $NUV$  magnitude, lies well above the BHB line (in (Fig. 9(b)) showing that its  $H\beta$  is too broad for it to be a BHB star.

### 7.4. Selection using the $(J-H)_0$ vs. $(H-K)_0$ Plot.

Brown et al. (2008) used the window  $-0.20 < (J-H)_0 < 0.10$  and  $-0.10 < (H-K)_0 < 0.10$  in making their initial selection of stars for the Century Survey. Fig. 10(a) shows the position of the local BHB stars (Kinman et al. 2000) in this diagram. These stars are concentrated in an area (outlined by the dotted rectangle) that is significantly smaller than the *CHSS* window (outlined by the dashed rectangle). Fig. 10(b) shows the same diagram for a sample of 24 BHB stars from the *CHSS* survey that have  $80^\circ \leq l \leq 100^\circ$  and  $-35^\circ \leq b \leq -55^\circ$ ; these stars are also contained by the dotted rectangle ( $-0.10 < (J-H)_0 < 0.15$  and  $-0.05 < (H-K)_0 < 0.09$ ). This confirms that this smaller window is adequate for selecting BHB stars. Fig. 10(c) shows the position of our *NR* survey BHB candidates in this diagram. Two stars, 41 and 162 have  $JHK$  colors that lie outside the window and consequently are hotter than the other BHB candidates.

### 7.5. The Selection of BHB Stars from the Candidates.

We make our final selection from the fifty four BHB candidates that are given in Table 5 where a weight is given to each star for each selection method according to the probability of its being a BHB star. For selection

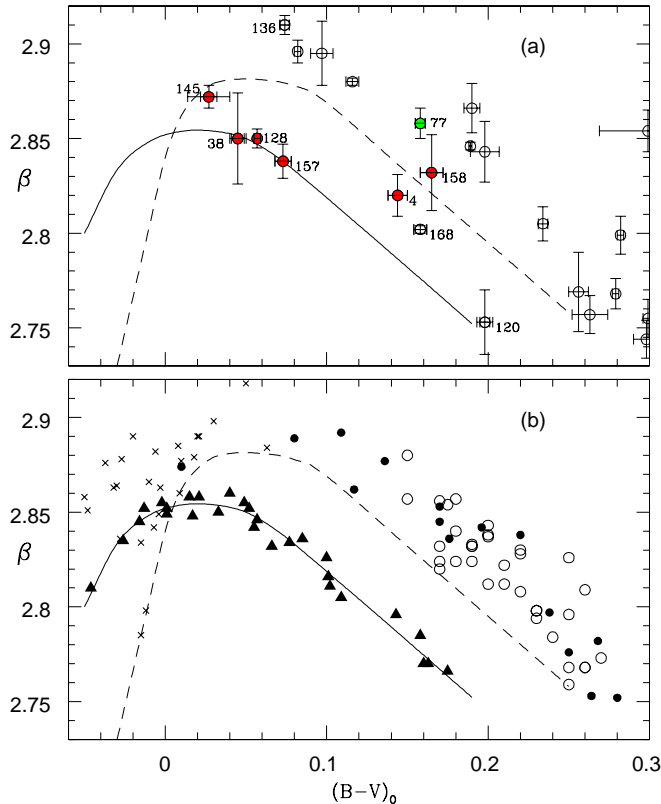


FIG. 9.— In both plots the ordinate is Strömgren  $\beta$  and the abscissa is Johnson  $(B - V)_0$ . In the lower figure 9(b), the local BHB stars are shown by filled triangles and their location is indicated by the solid curve. The data for these stars are taken from Kinman et al. (2000). The other symbols show the locations of nearby non-BHB stars and the lower limit of  $\beta$  for these stars is shown by the dashed line. The data for these non-BHB stars come from Gray & Garrison (1989) (open circles), Stetson (1991) (filled circles) and Crawford et al. (1972) (crosses). The solid and dashed curves are repeated in Fig. 9(a) which shows the locations of the program stars. The BHB candidates derived from the  $(u - B)_{K0}$  vs.  $(B - V)_0$  plot (Fig. 7) are shown by red and green filled circles. The other program stars are shown by open circles.

using  $(u - B)_{K0}$  and  $(NUV - V)_0$ , stars in the defining box were given weight +4; those whose error bars intersected the defining box were given weight +2. Others were given weights 0 and -3 according to their distance from the defining box. For selection using Strömgren  $\beta$ , stars on the defining line were given weight +3; others were given weight -3. For stars classified by the CHSS survey, those classified as BHB stars were given weight +4, the unclassified were given weight 0 and those with specific non-BHB classifications were given weight -4. We also included the 26 stars in the *NR* field that the *B2M* survey classifies as having a high (H) or medium (M) probability of being a BHB star. Weight 0 was given for this classification.

The weights from each selection method were added to give a total weight ( $W$ ) for each star. The fourteen stars with  $W \geq +6$  are classified BHB3 and are likely BHB stars. The seven stars with  $2 < W < 6$  are classified BHB2 and are possible BHB stars. The remaining thirty three stars with  $W \leq +2$  are classified BHB1 and are unlikely to be BHB stars. The mean properties of the stars in the three classes are given in Table 6.

## 8. DISCUSSION.

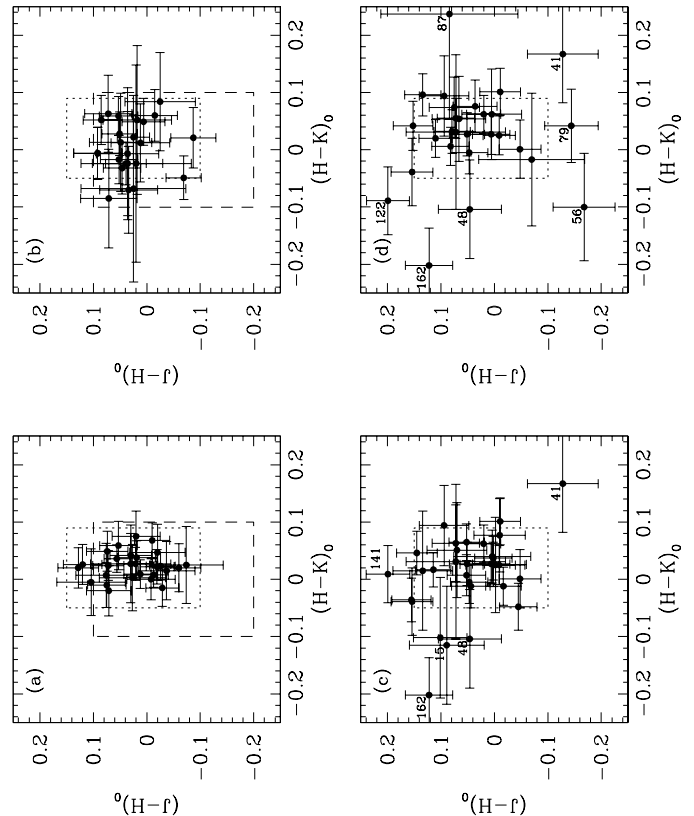


FIG. 10.— The 2MASS color  $(J - H)_0$  (ordinate) vs.  $(H - K)_0$  for (a) local BHB stars; (b) BHB stars from the *CHSS* sample (c) BHB candidates from *NR* field; (d) BHB candidates classified H and M in the *B2M* survey that are in the *NR* field. The significance of the dashed and dotted windows is given in the text. Stars that lie outside these windows are numbered.

We conclude that the 14 stars that we classified as BHB3 (Sec. 7.5) have a high probability of being BHB stars and that the 33 stars classified as BHB1 are unlikely to be BHB stars. BHB2 is an intermediate class whose nature needs clarification. The mean properties of these classes are given in Table 6; the stars in class BHB3 (the BHB stars) are fainter, bluer, more metal-poor and have a more negative radial velocity ( $RV_{lsr}$ ) than those in class BHB1 (the non-BHB stars). The ranges in these parameters are also smaller for the BHB stars. The Shapiro-Wilk test (Shapiro & Wilk, 1965) shows that the  $RV_{lsr}$  distribution of the BHB3 stars shows no departure from normality as we would expect for a kinematically homogeneous group. The  $RV_{lsr}$  distribution of those in BHB1, however, shows a very significant departure from normality. Evidently, the BHB1 class (non-BHB stars) contain both disk and halo stars (c.f. Fig 8. in Brown et al. (2008)).

The data in color-color plots are affected both by errors in the correction for interstellar extinction and also systematic errors in the photometric systems. It is not easy to evaluate such errors and so it is important to compare our results with those from other surveys that depend on other selection methods.

### 8.1. Comparison with *CHSS* and *B2M* surveys.

The *CHSS* survey has 10 stars that are in the *NR* survey area. They classify 3 of them as BHB stars in

TABLE 6  
PROPERTIES OF THE CLASSES OF BHB CANDIDATES.

Class <sup>a</sup>	N <sup>b</sup>	$\langle V_0 \rangle$ <sup>c</sup>	Range <sup>d</sup> in $V_0$	$\langle (B - V)_0 \rangle$ <sup>e</sup>	Range <sup>f</sup> in $(B - V)_0$	$\langle [m/H] \rangle$ <sup>g</sup>	Range <sup>h</sup> in $[m/H]$	$\langle RV_{lsr} \rangle$ <sup>i</sup> km s <sup>-1</sup>	Range <sup>j</sup> in $RV_{lsr}$
BHB3	14	13.91	2.69	+0.057	0.198	-1.41	3.00	-108±29	327
BHB2	07	13.60	3.06	+0.099	0.141	-1.27	2.60	-93±44	260
BHB1	33	13.43	4.42	+0.148	0.761	-1.13	2.70	-53±16	352

- <sup>a</sup> BHB Class as defined in Sec. 7.5  
<sup>b</sup> Number of stars in class.  
<sup>c</sup> Mean  $V_0$  for stars in class.  
<sup>d</sup> Range in  $V_0$  for stars in class.  
<sup>e</sup> Mean  $(B - V)_0$  for stars in class.  
<sup>f</sup> Range in  $(B - V)_0$  for stars in class.  
<sup>g</sup> Mean  $[m/H]$  for stars in class.  
<sup>h</sup> Range in  $[m/H]$  for stars in class.  
<sup>i</sup> Mean radial velocity corrected to LSR for stars in class.  
<sup>j</sup> Range in radial velocity corrected to LSR for stars in class.

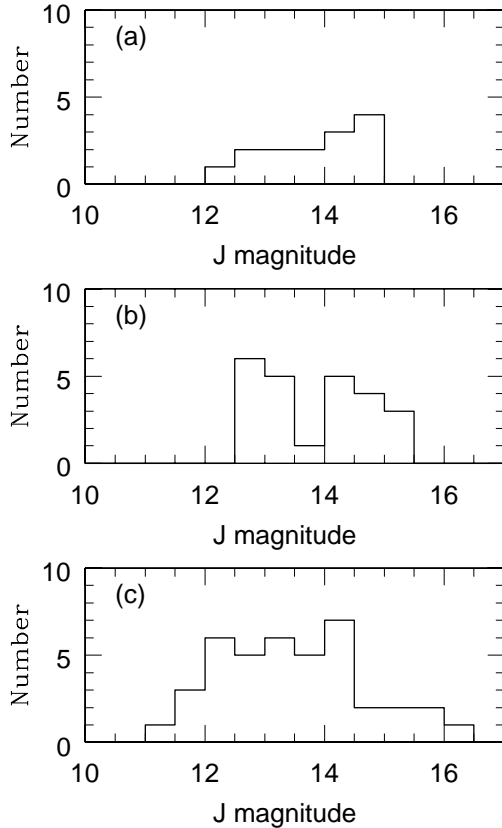


FIG. 11.— The distribution with 2MASS J magnitude of (a) The BHB stars classified as BHB3 in Table 5 (70 deg<sup>2</sup>). (b) Nearby sample of BHB stars in the *CHSS* survey (119 deg<sup>2</sup>). (c) Nearby sample of stars classified as “H” and “H:” (high probability of being BHB stars in the *B2M* survey (66 deg<sup>2</sup>).

agreement with our classification as BHB3. They either do not classify the remaining 7 or classify them as a type other than BHB; we call all these 7 class BHB 1. The *CHSS* survey covers an area of 119 deg<sup>2</sup> in the sky between  $80^\circ \leq l \leq 100^\circ$  and between  $-55^\circ \leq b \leq -35^\circ$ . In this field they classify 24 stars as type BHB and 6 as BHB/A. The corresponding surface densities are  $0.20 \pm 0.04$  and  $0.05 \pm 0.02$  stars deg<sup>-2</sup> respectively for the BHB and BHB/A types. In the *NR* field, the density

TABLE 7  
MEAN GALACTOCENTRIC RADIAL VELOCITIES AND THEIR DISPERSIONS FOR *CHSS* AND *NR* BHB STARS WITH GALACTIC LONGITUDES NEAR  $90^\circ$ .

Z range <sup>a</sup> kpc	$\langle Z \rangle$ <sup>b</sup> kpc	n <sup>c</sup>	Area Deg <sup>2</sup>	$V_{gal}$ <sup>d</sup> km s <sup>-1</sup>	$\sigma$ <sup>e</sup> km s <sup>-1</sup>
< 4	2.68	36	281	+34.9±15.9	94.2±11.1
> 4	5.78	25	281	+12.1±27.0	132.1±18.7

- <sup>a</sup> Range in Z.  
<sup>b</sup> Mean value of Z.  
<sup>c</sup> Number of BHB stars in Field.  
<sup>d</sup> Mean Galactocentric Velocity with error.  
<sup>e</sup> Dispersion in Galactocentric Velocity with error.

of the class BHB3 stars is  $0.19 \pm 0.05$  stars deg<sup>-2</sup> while that of type BHB2 is  $0.09 \pm 0.04$  stars deg<sup>-2</sup>. Although the *CHSS* survey extends to slightly fainter magnitudes (Fig. 11b), the *CHSS* BHB stars and our BHB3 stars have a similar magnitude range. There is therefore good agreement overall between the *CHSS* and our present survey.

The *B2M* survey has 26 stars that are classified H or H: and 3 as M that are in the *NR* survey area. Only 5 of these (4 class H and 1 class M) are in our class BHB3 and so are likely to be BHB stars while 17 (15 as H and H: and 2 as M) are in class BHB1 and so are unlikely to be BHB stars. To get a larger sample of the *B2M* survey in this part of the sky, we took those in the R.A. range 23:00 to 23:40 and Declination range  $+02^\circ$  to  $+20^\circ$ . Forty *B2M* stars in this region are classified as either H or H: and have a mean galactic longitude (l) of  $89^\circ$  and mean galactic latitude (b) of  $-47^\circ$ ; they are contained in an area of 66.2 deg<sup>2</sup>. This corresponds to  $0.60 \pm 0.10$  stars deg<sup>-2</sup> or three times the surface density of the BHB stars found by the *CHSS* and our survey. Some this excess may be caused by the *B2M* survey having a slightly deeper limiting magnitude but it is mainly caused by the inclusion of non-BHB stars. The *B2M* sample (Fig. 11c) contains many stars that are significantly brighter than those in the other two surveys. We conclude that only about a third to one half of the stars that *B2M* classify as having a high probability of being BHB stars are ac-

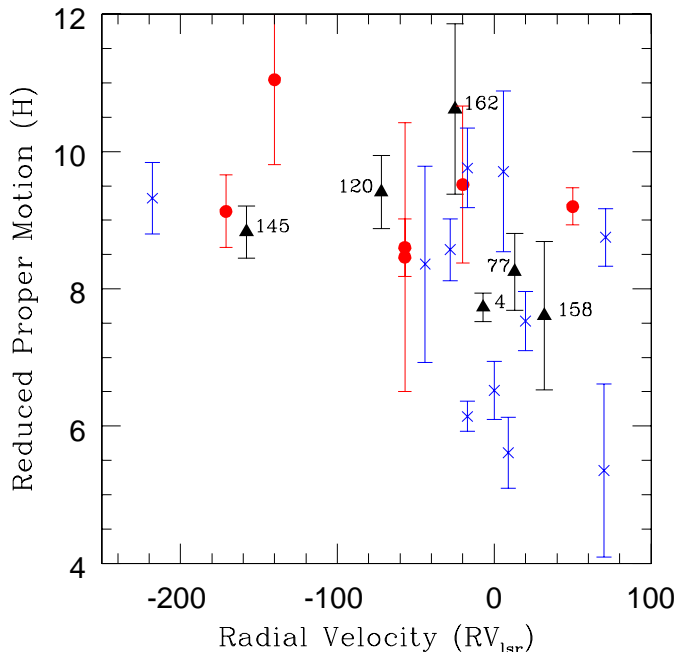


FIG. 12.— The reduced proper motion  $H$  (ordinate) vs. radial velocity in  $\text{km s}^{-1}$  ( $RV_{lsr}$  for stars of (a) class BHB3 (red filled circles), (b) class BHB2 (black filled triangles) and (c) class BHB1 (blue crosses).

tually BHB stars. This result is consistent with that of Ortiz et al. (2010) who made a spectroscopic survey of 43  $B2M$  stars. They found only 13 stars (30% of their sample) could be reliably identified as BHB stars, 25% could be identified as some other type and for 40% the type was uncertain. Many of the stars in their sample had  $(B - V)_0 \leq 0.0$  or  $T_{eff} \geq 10,000^\circ$  and the classification of such stars is difficult (Behr 2003).

In the Appendix C, we take larger samples of the *CHSS* and  $B2M$  BHB stars and examine the probabilities that they are BHB stars given by Smith et al. (2010). Many of the stars that  $B2M$  classify as having a high probability of being BHB stars are not in the Smith et al. catalog and are likely to be too blue for the  $B2M$  classification to be correct.

### 8.2. The Ambiguous class in the present sample.

The ambiguous class (BHB2) contains stars of two types. The first type (stars 60, 92 and 162) are relatively faint ( $V > 14$ ) stars for which the observations have too low a weight to assign them to class BHB3. Stars 60 and 92 have large negative  $RV_{lsr}$  and are likely to be halo stars, while star 162 has a low  $RV_{lsr}$  and a location on the  $(J - H)_0$  vs.  $(H - K)_0$  that differs from that of other BHB stars (Fig. 10(c)). The second type (stars 4, 120, 145, and 158 in BHB2 and 77 in BHB1) are those where the classification based on Strömgren  $\beta$  differs from that based on  $(u - B)_{K0}$  and/or  $(NUV - V)_0$ . These latter are brighter ( $V < 13.2$ ) and, except for star 145, have lowish  $RV_{lsr}$  and  $(B - V)_0 \geq 0.14$ .

The reduced proper motion  $H$  is defined (following Stetson 1981) by:

$$H = V_0 + 5 + 5 \log \mu \quad (3)$$

where  $V_0$  is the extinction-corrected  $V$  magnitude, and  $\mu$  is the *total* proper motion in arcsec per year. Fig. 12 is

a plot of  $H$  against the radial velocity of the 23 stars for which significant proper motions are available from the UCAC3 catalog (Zacharias 2010). The BHB stars (red filled circles) have a wide range of radial velocity but a restricted range of reduced proper motion ( $H$ ). A few of the non-BHB stars (blue crosses) are also found in the same location as the BHB stars but most have a broad range in  $H$  and a smaller  $V_{lsr}$  than the BHB stars. The ambiguous BHB2 class (black triangles) show an intermediate location and so their kinematics are as ambiguous as their other properties. We judge that among these stars, 60, 92, 120 and 145 are the most likely and 4, 77, 158 and 162 are the least likely to be BHB stars. Stars 60, 90, 120 and 145 have a mean  $RV_{lsr}$  of  $-118 \text{ km s}^{-1}$  and so their addition to our BHB3 sample of BHB stars would only change the mean velocity to  $-111 \pm 24 \text{ km s}^{-1}$ . The surface density of these 4 stars is  $0.06 \pm 0.03 \text{ deg}^{-2}$  which is similar to the surface density of  $0.05 \pm 0.02 \text{ deg}^{-2}$  for the BHB/A types of the *CHSS* survey.

We conclude that both the *CHSS* and our present survey are of similar quality. The selection criteria in both ensure that the stars which they classify as BHB stars have few interlopers. Both surveys, however, identify significant numbers of stars ( $\sim 25\%$  as many as in the BHB class) that have perhaps a 50% chance of being BHB stars. The sum of the BHB and BHB/A classes will therefore be more complete but  $\sim 10\%$  of its content will be misidentified.

### 8.3. Disk or Inner Halo BHB stars?

#### 8.3.1. Radial Velocities.

Radial velocity alone can be used to discriminate the population type at galactic longitudes  $90^\circ$  and  $270^\circ$ , and we consider the BHB stars in several fields with these galactic longitudes. The first field contains the 26 BHB stars in the *CHSS* with  $80^\circ < l < 100^\circ$  and  $+55^\circ < b < +35^\circ$ . The second field contains the 24 BHB stars in the *CHSS* with  $80^\circ < l < 100^\circ$  and  $-55^\circ < b < -35^\circ$ . The third field is the *NR* field that contains 14 BHB stars. Taking into account overlapping, there are 61 BHB stars in these fields; their mean galactocentric radial velocities and their dispersions and other properties are given in Table 7.

If a significant fraction of the BHB stars belong to the disk, we expect that BHB stars with  $Z < 4 \text{ kpc}$  will have more positive galactocentric radial velocities and smaller radial velocity dispersions than those with  $Z > 4 \text{ kpc}$ . If such an effect is present in the sample in Table 7, it is at the limit of significance. Disk BHB stars should not have a normal radial velocity distribution. Application of the Shapiro-Wilks test to the 36 BHB stars in the  $Z < 4 \text{ kpc}$  and the 17 BHB stars with  $Z < 2.5 \text{ kpc}$  in our sample give  $W = 0.951$  and  $0.923$  respectively; neither sample shows a significant departure from a normal distribution.

The evidence from the radial velocities therefore suggests that any disk component of the BHB stars must be quite small; this agrees with the previous analysis of the proper motions of *CHSS* BHB stars by Kinman et al. (2009). For stars with  $Z < 4 \text{ kpc}$ , there is some evidence that the BHB stars show slightly prograde rotation (c.f. Carollo et al. 2007<sup>5</sup>). but for  $Z > 4$ , there is no evidence for rotation; this agrees with the analysis of the

<sup>5</sup> For a criticism of this paper, however, see Schönrich et al.



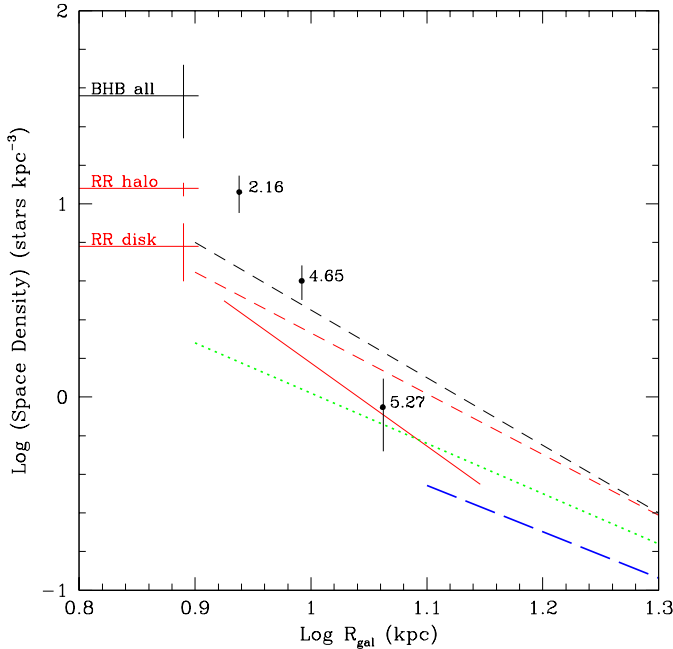


FIG. 13.— The ordinate is the Log of the space density in stars  $\text{kpc}^{-3}$  and the abscissa is the Log of the Galactocentric distance in kpc. The black filled circles refer to the BHB stars described in Table 7 and the numbers beside them give their mean height  $\langle Z \rangle$  from the Galactic plane (in kpc). The black dashed line is for a spherical halo of BHB stars with  $Z > 5$  kpc and is taken from Kinman et al. (1994). The green dotted line shows the extrapolation of the BHB space densities for the Northern field of De Propris et al. (2010). The blue line (long dashes) shows the BHB space densities of their Southern field. The red solid line shows the *QUEST* RRab Lyrae space densities (Vivas & Zinn, 2006) and the red dashed line shows the *LONEOS* RRab Lyrae space densities (Miceli et al. 2008). The local space densities of the BHB and RR Lyrae stars are from Kinman et al. (2009).

motions of 1700 subdwarfs in the contiguous Stripe 82 field (Smith et al. 2009).

### 8.3.2. Space Densities.

The space densities of halo stars are generally represented in terms of a power-law of the galactocentric distance ( $R_{\text{gal}}$ ) and a flattening which may either be constant or a function of  $R_{\text{gal}}$  such as that introduced by Preston et al. (1991). Recent estimates of the power-law exponent and the flattening ( $c/a$ ) vary quite widely (see Table 2 in Miceli et al. (2008)). The older studies tended to find steeper exponents such as the  $-3.2$  and  $-3.5$  for RR Lyrae stars and BHB stars respectively by Preston et al. (1991), the  $-3.5$  found for BHB stars with  $Z > 5$  kpc by Kinman et al. (1994) and the  $-3.53$  for RR Lyrae stars by Wetterer and McGraw (1996). More recently Miceli et al. used their *LONEOS* RR Lyrae survey to model a spherical halo with exponents of  $-2.26 \pm 0.07$  for Oosterhoff Type I RR Lyrae stars and  $-2.88 \pm 0.11$  for those of Oosterhoff type II. They also found a model with variable flattening for both Oosterhoff types with an exponent of  $-3.15 \pm 0.07$ . A similar exponent ( $-3.1$ ) was found by Vivas and Zinn (2006) from their *QUEST* RR Lyrae survey using a model with variable flattening that excludes regions that have pronounced overdensities. We consider the *LONEOS* and *QUEST* surveys

(2010).

(which refer only to type *ab* RR Lyrae stars) to be the most reliable now available. The *LONEOS* space densities have been recomputed for an RR Lyrae  $M_V$  of  $+0.55$  (as used by Vivas & Zinn) and are shown by red dashed lines in Fig. 13. The *QUEST* space densities are shown by a full red line in this figure. Both surveys predict a space density of 5 RRab stars  $\text{kpc}^{-3}$  at the solar  $R_{\text{gal}}$  of 8.0 kpc. This is appreciably less than the observed local density for both disk and halo type *ab* RR Lyraes ( $14 \pm 2$  stars  $\text{kpc}^{-3}$ ) which itself is likely to be a lower limit. About a third of these local stars are the disk RR Lyrae stars that are more metal-rich than the halo RR Lyraes and which have different kinematics, but there are still about twice as many local *halo* type *ab* RR Lyrae stars as would be predicted by the *LONEOS* and *QUEST* surveys<sup>6</sup>.

We calculate space densities ( $\rho$ ) in stars  $\text{kpc}^{-3}$  for the BHB stars near galactic longitude  $90^\circ$  (Table 7) for three volume elements bounded by distances of 0.0, 4.0, 6.5 and 8.5 kpc in which the survey is thought to be complete. These are shown in a plot of  $\log \rho$  vs.  $\log R_{\text{gal}}$  in Fig. 13 where the mean height above the plane ( $|Z|$ ) of each volume element is shown next to the corresponding space density. Also plotted are the space densities of the local BHB and RR Lyrae stars (Kinman et al. 2009). Fig. 13 may be compared with a similar plot (Fig. 15 in Kinman et al. 1994) where both BHB stars and RR Lyraes have comparable space densities that (for  $Z > 5$  kpc) could be represented by a spherical halo with a power law exponent of  $-3.5$  (shown by the black dashed line in Fig. 13). De Propris et al. (2010) found exponents of  $-2.6$  and  $-2.4$  for spherical halo fits to the Northern and Southern fields of their BHB survey (shown in Fig. 13 by green dotted lines and long blue dashed lines for their Northern and Southern fields respectively). Their Northern field lies on the celestial equator with an R.A. between  $09^h 30^m$  and  $14^h 30^m$  and their Southern field covers the South Galactic Pole. The outermost point ( $|Z| = 5.27$  kpc) for our sample of BHB stars near galactic longitude  $90^\circ$  is in good agreement with an *extrapolation* of the power-law which they fit to the space densities of their Northern field. Our two innermost points for  $|Z| = 2.16$  and  $4.65$ , however, are much larger than the predictions of these models and show that  $\rho$  increases towards the galactic plane more steeply than they predict from analyses of stars in the outer halo; this is also shown by Kinman et al. (1994) in their Fig. 15.

We know, however, both from the kinematics of local BHB stars, from our present analysis of the radial velocities of BHB stars with galactic longitudes near  $90^\circ$ , and from the proper motion analysis of CHSS stars at the North Galactic Pole (Kinman et al. 2009) that this excess of BHB stars near the plane has a disk-like spatial distribution but is largely composed of stars that have zero or low galactic rotation. We conclude that the BHB stars are revealing a spatially flattened, non-rotating “inner halo” as described by Kinman et al. (2009) and Morrison et al. (2009).

<sup>6</sup> We noted in Sec. 4.2 that the surface densities of the RR Lyrae stars that we find in the *NR* field roughly agree with those found in the *LONEOS* survey if we take into account that only the higher amplitude variables are found in the *ASAS-3* and *NSVS* surveys.

## 9. CONCLUSION.

The distribution of heliocentric radial velocities  $V_{hel}$  of the early-type stars in the *SR* field of Rodgers et al. (1993a) ( $l = 270^\circ$ ,  $b = -45^\circ$ ) does not show any evidence for the anomalous disk of faint turn-off stars found by Gilmore et al. (2002) in the same galactic location. There is a peak in these *SR* velocities, however, that corresponds to the slightly prograde galactocentric radial velocity of  $-30 \text{ km s}^{-1}$ . These stars are listed and discussed in Appendix A; it is unlikely that more than a third of these stars could be BHB stars. There is little evidence for a corresponding peak in the radial velocities in the *NR* field. The mean galactocentric radial velocity of the BHB stars near galactic longitude ( $l$ ) =  $90^\circ$  that have  $Z < 4 \text{ kpc}$  (Table 7) may be slightly prograde but the Shapiro-Wilk test shows that this group has a normal distribution and so is likely to consist of a homogeneous group of halo stars rather than a mix of disk and halo stars. The BHB stars in Table 7 with  $Z > 4 \text{ kpc}$  show no rotation.

New photometry and supplementary data for the early-type stars in the *NR* field are given in Table 1 of this paper. Plots of  $(u - B)_{K0}$  vs.  $(B - V)_0$ ,  $(NUV - V)_0$  vs.  $(B - V)_0$ , and Strömgren  $\beta$  vs.  $(B - V)_0$  are used to indicate the probability that they are BHB stars. Amongst those with the appropriate  $(B - V)_0 < 0.20$ , 14 have a high probability of being BHB stars and 33 are unlikely to be BHB stars. The classification of 8 is ambiguous but further study shows that only 4 of these are likely to be BHB stars. There are 10 stars in the *CHSS* Century survey that are in the *NR* field; 3 are classified as BHB stars in both our and the *CHSS* surveys. We classify the other 7 stars as unlikely to be BHB stars and they are either given non-BHB types or are unclassified in the *CHSS* survey. The surface densities (stars  $\text{deg}^{-2}$ ) in both our survey of the *NR* field and that of an adjoining *CHSS* field show good agreement in completeness between the two surveys. This is not true of the *B2M*

survey where about three quarters of the 26 stars which Beers et al. (2007b) classify as likely to be BHB stars are classified by us as non-BHB stars. Smith et al (2010) have used *SDSS* colors to assign probabilities for stars in the *DR7* release to be BHB stars. There is fair agreement between our classifications and these probabilities for the 5 stars in our survey that are faint enough to be included in their catalog. A comparison of the Smith et al. probabilities with a sample from the *CHSS* survey indicates, however, that the use of the *SDSS* colors alone can only isolate a sample that is about 80% pure.

Among the early-type stars in the *NR* field, we identify three type *ab* RR Lyrae variables with mean  $V$  magnitudes brighter than 15 (the approximate limit of the BHB survey). New photometric and spectroscopic data are given for these stars. A fourth type *ab* RR Lyrae has been found in the field by Kinemuchi (2006). Its  $V$  magnitude is  $\sim 15$ . A fifth type *ab* field RR Lyrae of lower amplitude was found in the field by the *LONEOS* survey but was not found by the *NSVS* because of confusion with brighter stars. We estimate from the *LONEOS* survey that there should be 7 type *ab* RR Lyraes in the *NR* field or about half of the number of BHB stars.

We thank Dr. Nick Suntzeff for kindly making available the radial velocities of 18 early-type stars in the *NR* survey. This research has made use of the VizieR catalog access tool, CDC, Strasbourg, France and 2MASS data provided by the NASA/IPAC Infrared Science Archive, which is operated by the Jet Propulsion Laboratory, California Institute of Technology, under contract with NASA. Use was also made of MAST (Multimission Archive at the STScI which is operated for NASA by AURA), the SIMBAD database (operated at the CDS, Strasbourg, France), ADS (the NASA Astrophysics Data System) and the Astro-ph e-print server. Finally we would like to thank the referee for a careful reading of this text that has enabled us to make a number of corrections and clarifications.

## REFERENCES

- Abazajian, K. et al., 2009, ApJS, 182, 543  
Allard, F., Wesemael, F., Fontaine, G., Bergeron, P., Lamontagne, R. 1994, AJ, 107, 1565  
Beers, T.C. 1990, AJ, 99, 323  
Beers, T., Preston, G., Szechtman, S., 1988 ApJS, 67, 461  
Beers, T., Wilhelm, R., Doinidis S., Mattson, C. 1996, ApJS, 103, 433  
Beers, T., Chiba, M., Yoshii, Y., Platais, I. et al. 2000, AJ, 119, 2866  
Beers, T., Flynn, C., Rossi, S. et al. ApJS, 168, 128  
Beers, T., Almeida, T., Rossi, S., Wilhelm, R., Marsteller, B. 2007, ApJS, 168, 277  
Behr, B.B. 2003, ApJS, 149, 101  
Belokurov, V., Evans, N., Bell, E., Irwin, M., Hewitt, P. et al. 2007, ApJL, 657, L89  
Bell, E., Xue, X., Rix, H.-W., Ruhland, C. Hogg, D. 2010, AJ, 140, 1850  
Brown, W.R., Geller, M.J., Kenyon, S.J., et al. 2004, AJ, 127, 1555  
Brown, W.R., Beers, T.C., Wilhelm, R., Allende Prieto, C., Geller, M.J., Kenyon, S.J., Kurtz, M.J. 2008, AJ, 135, 564  
Brown, W.R., Geller, M.J., Kenyon, S.J., Diaferio, A. 2010 AJ, 139, 59  
Carollo, D., Beers, T., Lee, Y., Chiba, M. et al. 2007, Nature, 450, 1020  
Carollo, D., Beers, T., Chiba, M., Norris, J. et al. 2010, ApJ, 712, 692  
Clementini, G., Gratton, R., Bragaglia, A., Carretta, E. et al. 2003, AJ, 125, 1309  
Clewley, L., Warren, S.J., Hewett, P.C. et al., 2002, MNRAS, 337, 87  
Crawford, D., Barnes, J., Gibson, J., Golson, J. et al. 1972, A&AS, 5, 109  
De Propriis, R., Harrison, C., Mares, P. 2010, ApJ, 719, 1582  
Dalessandro, E., Salaris, M., Ferraro, F., Cassisi, S. et al., 2010, MNRAS, 410, 694  
Deason, A., Belokurov, V., Evans, N. 2010, MNRAS tmp 1761D (astro-ph 1008.3067)  
Eggen, O.J., 1968, ApJS, 16, 97  
Eggen, O.J., Greenstein, J.L., 1965, ApJ, 141, 83  
For, B.-Q., Sneden, C. 2010, AJ, 140, 1694  
Gettel, S., Geske, M., McKay, T., 2006, AJ, 131, 621  
Gilmore, G., Wyse, R., Norris, J.E. 2002, ApJL, 574, L39  
Goranskij, 1986, Perem. Zvezdy. Byull., 22, 353  
Gray, R., Garrison, R. 1989, ApJS, 70, 623  
Horne, J., Baliunas, S. 1986, ApJ, 302, 757  
Kinemuchi, K., Smith, H., Wozniak, P., McKay, T., 2006, AJ, 132, 1202  
Kinman, T.D., Carretta, E. 1992 PASP, 104.111  
Kinman, T.D., Suntzeff, N.B., Kraft, R.P., 1994, AJ, 108, 1722  
Kinman, T.D., Pier, J.R., Suntzeff, N.B. et al. 1996, AJ, 111, 1164



- Kinman, T.D., Castelli, F., Cacciari, C., et al. 2000, A&A, 364, 102
- Kinman, T.D., Cacciari, C., Braggaglia, A., Buzzoni, A., Spagna, A. 2007a, MNRAS, 375, 1381
- Kinman, T.D., Salim, S., Clewey, L., 2007b, ApJL, 662, L111
- Kinman, T.D., Morrison, H.L., Brown, W.R. 2009, AJ, 137, 3198
- Kinman, T.D., Brown, W.R. 2010, AJ, 139, 2014
- Knude, J. 1997, A&A, 327, 90
- Kondo, M., Watanabe, E., Yutani, M., Noguchi, T. 1982, PASJ, 34, 541
- Landolt, A. 1992, AJ, 104, 340
- Lasker, B., Sturch, C., McClean, B., Russell, J., Jenkner, H., Shara, M., 1990, AJ, 99, 2019
- Lasker, B., Lattanzi, M., McClean, B. et al., 2008, AJ, 136, 735
- Liu, T. 1992, PASP, 103, 205
- Miceli, A., Rest, A., Stibbs, C., Hawley, S. et al. 2008, ApJ., 678, 865 (LONEOS Survey)
- Minchev, I., Quillen, A., Williams, M. Freeman, K., et al. 2009, MNRAS, 396, 56
- Möhlér, S. 2004 in IAU Symposium, Vol. 224, The A-Star Puzzle, ed. J. Zverko, J. Ziznovsky, S.J. Adelman, W.W. Weiss, 395-402
- Monet, D., Levine, S., Casian, B. et al. 2003, AJ, 125, 984 (USNO-B 1.0 catalog)
- Morrison, H., Helmi, A., Sun, J., Liu, P. et al. 2009, ApJ, 694, 130
- Morrissey, P., Conrow, T., Barlow, T., Small, T. 2007, ApJS, 173, 682
- Navarro, J., Helmi, A., Freeman, K. 2004, ApJL, 601, L43
- Norris, J., Ryan, S., Beers, T. 1999, ApJS, 123, 639
- Ortiz, R., Wilhelm, R., Costa, R., Rossi, S. et al., AJ, 139, 1031
- Pier, J.R. 1983, ApJS, 53, 507
- Pojmański, G. 2002, Acta Astr., 52, 397
- Preston, G.W. 1959, ApJ, 130, 507
- Preston, G.W., Shectman, S.A., Beers, T.C., 1991, ApJ, 375, 121
- Preston, G.W., Beers, T.C., Shectman, S.A. 1994, AJ, 108, 538
- Reid, M., Brunthaler, A. 2004 ApJ, 616, 872
- Rodgers, A. 1971, ApJ, 165, 581
- Rodgers, A., Roberts, W., Walker, I., 1993a, AJ, 106, 591
- Rodgers, A., Roberts, W., 1993b, AJ, 106, 1839
- Rodgers, A., Roberts, W., 1993c, AJ, 106, 2294
- Sandage, A.R., 1990, ApJ, 350, 603
- Sandage, A.R., 2004, AJ, 128, 858
- Schönrich, R., Asplund, M., Casagrande, L. 2010, astro-ph 1012.0842
- Searle, L., Rodgers, A. 1966, ApJ, 143, 809
- Shapiro, S., Wilk, M. 1965, Biometrika, 52, 591
- Schlegel, D., Finkbeiner, D. & Davis, M., 1998, ApJ, 500, 525
- Smith, M., Evans, N., Belokurov, V., Hewitt, P. 2009, MNRAS, 399, 1223
- Smith, K., Bailer-Jones, C., Klement, R., Xue, X., 2010, A&A, 522, 88
- Stetson, P., 1981, AJ, 86, 1337
- Stetson, P., 1991, AJ, 102, 589
- Suntzeff, N., Kraft, R., Kinman, T., 1994, ApJS, 93, 27
- Tody, D., Davis, L. 1992, ASP Conf. Ser. 25, Astronomical Data Analysis Software & Systems I, ed. D. Worrall, C. Biemesderfer, & J. Barnes (San Francisco: ASP), 484
- Watkins, L., Evans, N., Belokurov, V., Smith, M., Hewitt, P. 2009, MNRAS, 398, 1757
- Wegner, G. 1983, AJ, 88, 109
- Wegner, G., Africano, J., Goodrich, B., 1990, AJ, 99, 1907
- Wetterer, C., McGraw, J., Hess, T. Grashuis, R. 1996, AJ, 112, 742
- Wils, P., Lloyd, C., Bernhard, K. 2006, MNRAS, 368, 1757
- Woźniak, P., Vestrand, W., Akerlof, C., Balsano, R. et al., 2004, AJ, 127, 2436 (NSVS)
- Vivas, A.K., Zinn, R. 2006, AJ, 132, 714 (QUEST Survey)
- Xue, X., Rix, H.-W., Zhao, G., Re Fiorentin, P. et al., 2008, ApJ, 684, 1143
- Zacharias N., Finch, C., Girard, T. Hambly, N., Wycoff, G. et al. 2010, AJ, 139, 2184 (UCAC3 Catalog)

## APPENDIX

### A. THE SOUTHERN FIELD *SR* OF RODGERS ET AL. (1993A).

Fig. 14 shows the distribution of galactocentric radial velocities ( $V_{gal}$ ) for the early type stars in the *SR* field (above) and *NR* field (below).  $V_{gal}$  was calculated from the heliocentric radial velocity  $V_{hel}$  following Xue et al. (2008)<sup>7</sup>:

$$V_{gal} = V_{hel} + 10 \times \cos l \cos b + 225 \times \sin l \cos b + 7 \times \sin b \quad (A1)$$

The *SR* field has the same galactic coordinates  $(l, b) = (270, -45)$  as the field of Gilmore et al. (2002) but does not show evidence for an anomalous disk in its radial velocity distribution. The *SR* field does, however, show a peak around  $+125 \text{ km s}^{-1}$  in its velocity distribution. This shows up as a peak around  $-30 \text{ km s}^{-1}$  in its galactocentric radial velocity distribution. A similar peak may be present at  $+30 \text{ km s}^{-1}$  in the *NR* field but it is certainly much less pronounced than the peak in the *SR* field.

There are 24 stars in the *SR* field in the velocity range that covers this peak ( $-05 < V_{gal} < -50 \text{ km s}^{-1}$ ). They are listed in Table 8 with their proper motions and positions taken from the *UCAC3* catalog (Zacharias et al. 2010). This table gives the reduced proper motion (*H*) (defined by equation (3) in Sec. 8.2) for each star. We know from our study of the BHB stars in the *NR* field that BHB stars have an *H* that is roughly in the range 8.5 to 11.5. There are 8 to 10 stars in this range (depending on whether one also takes the Ca II K- line equivalent width into account). This is an upper limit to the number of BHB stars in this velocity range because non-BHB stars can also have *H* in this range. We conclude that the peak at  $-30 \text{ km s}^{-1}$  in  $V_{gal}$  must primarily be caused by non-BHB stars.

### B. ADDITIONAL DATA FOR STARS IN THE *NR* FIELD.

#### B.1. Improved positions for the fainter stars in the *NR* Field.

The positions given in Rogers et al. (1993a) are generally good to a few arcsec and therefore adequate for identification. A number of the fainter stars, however, had poorer positions and the coordinates of them (taken from the USNO-B 1.0 catalog (Monet et al. 2003)) are given in Table 9.

#### B.2. The *B2M* Survey.

Beers et al. (2007b) list a number of BHB candidates in the area of sky of the *NR* survey that are not listed by Rodgers et al. (1993a). They are mostly either too faint or too red to have been included in the *NR* survey; they are listed in Table 10.

<sup>7</sup> In this paper we adopt a solar galactocentric distance of 8.0 kpc (Reid & Brunthaler 2004) but an LSR circular velocity velocity of  $220 \text{ km s}^{-1}$  rather than their somewhat higher value of  $236 \pm 15$

$\text{km s}^{-1}$  to maintain compatibility with other recent work.

TABLE 8  
STARS IN RODGERS ET AL. *SR* FIELD WITH GALACTOCENTRIC RADIAL VELOCITIES IN RANGE  $-05$  TO  $-50$   $\text{km s}^{-1}$ .

No. <sup>a</sup>	ID <sup>b</sup>	RA (2000J)	Dec (2000J)	$RV_{lsr}$ <sup>c</sup> $\text{km s}^{-1}$	$RV_{gal}$ <sup>d</sup> $\text{km s}^{-1}$	$\mu_{\alpha}$ <sup>e</sup> (mas)	$\mu_{\delta}$ <sup>f</sup> (mas)	H <sup>g</sup>	ST <sup>h</sup>	$V$ <sup>i</sup> (mag.)	$W_0(K)$ <sup>j</sup> Å
001	P83l-10	03:08:48.54	-67:51:28	+113	-29	+18.4±1.8	-34.0± 1.8	12.3	A2	14.5	1.4
011	P83l-16	03:15:09.98	-66:07:50	+115	-27	+04.2±2.8	-09.1± 2.8	09.9	A1	15.2	0.2
027	P83l-18	03:21:19.12	-66:18:06	+109	-35	+07.7±2.8	+04.4± 2.5	08.6	A4	14.2	3.3
029	P83s-44	03:22:34.13	-63:39:46	+102	-40	+01.8±1.7	-43.4± 1.7	11.4	F3	13.3	5.6
030	P83l-19	03:22:37.99	-66:21:33	+123	-21	+06.5±2.8	+01.5± 3.4	08.4	A0	15.0	1.4
050	P117l-10	03:26:30.21	-60:18:49	+120	-19	+12.0±13.2	-18.9± 2.0	10.5	A0	14.3	0.0
053	P117l-22	03:26:57.10	-58:04:26	+107	-30	+33.4±2.4	+23.2± 2.5	13.0	A0	15.1	2.3
072	P83l-54	03:31:38.22	-64:07:37	+134	-11	+05.9±2.5	-06.0± 2.5	09.4	A0	15.1	0.7
077	P117l-12	03:33:28.30	-59:40:29	+097	-44	+03.3±2.3	+02.1± 2.2	06.3	A4	14.6	3.2
080	P117l-30	03:34:34.82	-57:49:17	+098	-41	+07.5±1.8	-01.1± 1.7	09.2	A0	15.0	0.0
081	P83l-77	03:34:21.13	-62:05:56	+117	-27	-00.1±2.3	-02.9± 1.8	<7	A2	15.0	2.4
091	P83l-76	03:39:22.53	-63:28:58	+109	-37	+08.9±2.0	-07.4± 2.1	10.4	A1	15.2	1.0
093	P83l-73	03:42:02.58	-63:18:57	+111	-36	+03.8±2.0	+04.6± 1.6	07.9	A0	14.3	0.3
099	P117l-35	03:44:57.82	-56:41:52	+123	-19	+06.2±2.5	-03.0± 6.6	<8	A0	14.7	0.7
106	P117s-20	03:45:56.92	-61:19:11	+104	-42	+23.2±1.2	+08.8± 1.8	08.8	A0	11.9	0.0
111	P83l-70	03:47:10.41	-63:17:27	+125	-23	-05.4±1.4	+00.6± 1.4	06.8	A1	13.4	0.0
129	P117l-44	03:52:18.28	-59:25:24	+112	-35	+12.0±5.8	-19.7± 5.8	10.3	A1	13.7	0.4
145	P83l-29	03:58:00.27	-66:27:09	+104	-49	+02.2±4.4	+00.8± 2.5	<8	A0	15.3	0.0
147	P83s-23	03:58:12.55	-66:29:41	+103	-50	+20.7±1.2	+03.8± 1.0	08.4	A4	11.9	2.1
159	P83l-37	04:00:43.48	-64:15:34	+134	-19	+00.3±2.2	+01.1± 2.4	<7	A0	14.8	0.6
167	P117l-66	04:04:19.67	-59:47:24	+130	-21	+08.0±1.2	-00.7± 1.5	06.6	A0	12.2	0.0
180	P83l-38	04:05:42.79	-64:26:47	+142	-12	+04.8±1.8	-02.9± 1.8	07.3	A2	13.9	0.0
182	P83l-31	04:07:05.52	-65:34:30	+126	-29	+06.5±2.5	-00.6± 2.6	08.9	A1	15.3	0.3
184	P83l-36	04:07:26.79	-64:44:57	+109	-46	-01.6±2.4	+01.6± 7.0	<8	A1	15.0	0.3

<sup>a</sup> Number from Rodgers et al. (1993)

<sup>b</sup> ID from Rodgers et al. (1993)

<sup>c</sup> Radial Velocity corrected to LSR from Rodgers et al. (1993a).

<sup>d</sup> Galactocentric Radial Velocity.

<sup>e</sup> Proper Motion in R.A. from UCAC3 (Zacharias et al. 2010)

<sup>f</sup> Proper Motion in Dec. from UCAC3 (Zacharias et al. 2010)

<sup>g</sup> Reduced Proper Motion (Equation (3) in Sec 8.2).

<sup>h</sup> Spectral Type from Rodgers et al. (1993a).

<sup>i</sup>  $V$  magnitude from Rodgers et al. (1993a).

<sup>j</sup> Ca II K-line Eq. Width corrected for an interstellar component according to Rodgers et al. (1993a).

<sup>k</sup> H $\delta$  Eq. Width from Rodgers et al. (1993a).

TABLE 9  
COORDINATES FOR THE FAINTER STARS IN THE  
*NR* FIELD.

No.	ID	RA (2000J)	Dec (2000J)
18	Pn231l-11	23:11:23.8	+09:58:46
25	Pn23s1-13	23:12:21.6	+10:47:03
60	Pn24l-42	23:18:13.1	+08:38:08
63	Pn23l2-2	23:18:34.5	+13:51:26
72	Pn23l2-4	23:20:07.8	+12:37:47
75	Pn24l-13	23:20:47.0	+05:11:43
83	Pn24l-16	23:21:47.7	+07:50:56
87	Pn23l2-35	23:22:20.8	+12:06:59
89	Pn23l1-28	23:22:25.8	+11:47:56
92	Pn23l1-29	23:22:34.1	+12:05:08
104	Pn23l2-58	23:24:38.2	+07:51:02
121	Pn23l2-27	23:26:25.2	+12:46:19
122	Pn23l2-55	23:26:37.9	+08:35:26
123	Pn24l-24	23:26:37.7	+08:36:10
124	Pn24l-21	23:26:44.6	+06:17:42
138	Pn24l-5	23:28:47.9	+05:14:55

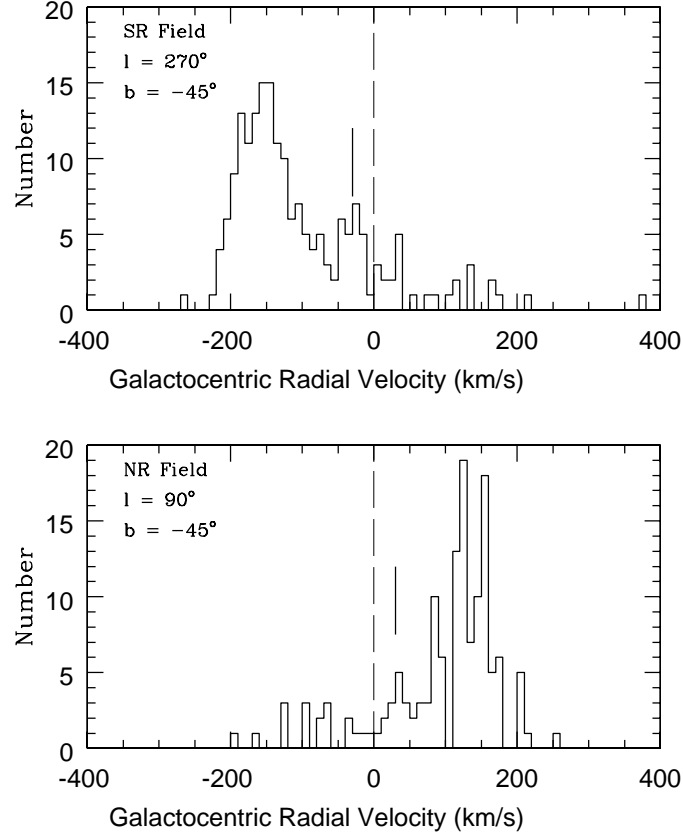


FIG. 14.— Distribution of the galactocentric radial velocities ( $V_{gal}$ ) in  $\text{km s}^{-1}$  for the *SR* (above) and *NR* (below) fields. The vertical dashed line at ( $V_{gal} = 0.0$ ) is the expected mean velocity for halo stars. The short vertical bars show the location of the peak in the *SR* field and its equivalent location in the *NR* field.

TABLE 10  
BHB CANDIDATES IN *B2M* SURVEY THAT ARE NOT IN *NR* SURVEY.

ID <sup>a</sup> BPS	$V_{20}$ <sup>b</sup> (mag.)	$(B - V)_{20}$ <sup>c</sup> (mag.)	RA (2000J)	Dec (2000J)	Probability <sup>d</sup>
CS 30338-100	13.96	0.637	23:13:51.5	+09:27:25	L
CS 30338-104	15.09	0.050	23:14:14.5	+11:10:33	H
CS 30338-097	13.78	0.464	23:15:54.0	+07:43:14	L:
CS 30338-098	12.13	0.490	23:17:05.0	+07:41:15	L
CS 30338-091	15.54	-0.020	23:17:11.4	+09:55:49	H
CS 30338-081	13.75	0.501	23:18:01.9	+08:40:17	L
CS 30338-053	14.19	0.365	23:21:21.4	+07:20:35	M
CS 30338-059	13.84	0.564	23:23:02.7	+10:19:28	L
CS 30338-061	14.02	0.779	23:23:14.9	+11:54:30	L
CS 30338-047	12.81	0.416	23:25:21.8	+10:41:15	L
CS 30338-028	14.62	0.674	23:25:29.3	+08:59:50	L
CS 30338-033	14.80	0.551	23:25:57.6	+09:45:54	L
CS 30338-015	15.73	0.103	23:28:12.3	+10:59:47	H
CS 30338-005	12.45	0.717	23:31:02.7	+08:34:51	L
CS 29522-103	13.54	0.487	23:32:02.1	+10:52:13	L
CS 31088-091	14.56	-0.052	23:33:58.1	+04:03:58	H
CS 30333-112	14.76	0.399	23:34:34.4	+09:08:25	M
CS 30338-100	13.96	0.637	23:28:47.9	+05:14:55	L

<sup>a</sup> ID from Beers et al. (1988)

<sup>b</sup> Dereddened  $V$  magnitude from from Beers et al. (2007b)

<sup>c</sup> Dereddened  $(B - V)$  magnitude from from Beers et al. (2007b)

<sup>d</sup> Probability that candidate is BHB star (Beers et al. (2007b) (H = High; M = Medium; L = Low)

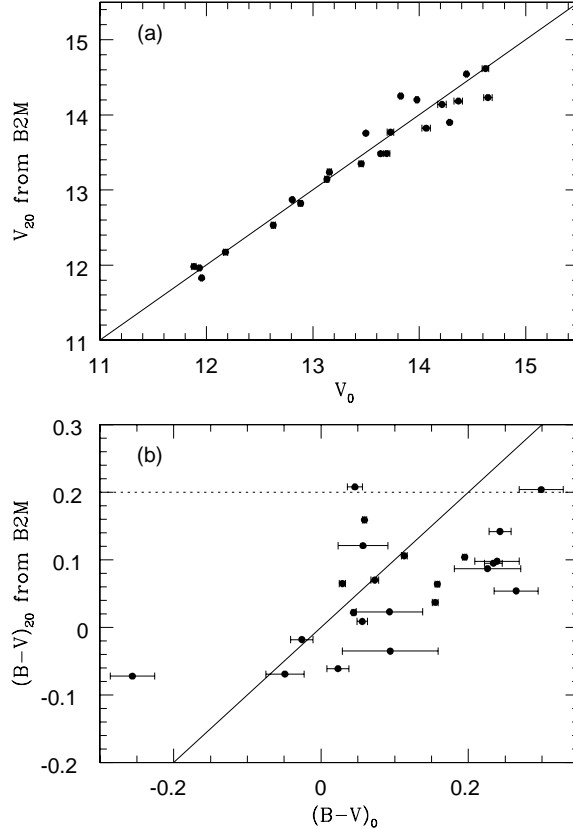


FIG. 15.— A comparison of our  $V_0$  and  $(B-V)_0$  with the  $V_{20}$  and  $(B-V)_{20}$  given by Beers et al. (2007b) in their *B2M* survey. The horizontal dashed line in Fig. 15 (b) is the *B2M* red limit of  $(B-V)_{20}$  for the star to have a high probability of being a BHB star.

### B.3. Miscellaneous Data for Stars in the *NR* field from Rodgers et al. (1993b).

The spectrophotometry and radial velocities of the stars with spectral types earlier than F0 given in Table 1 of Rodgers et al. (1993b) are available electronically but may not be easily accessible to all readers. We have therefore reproduced these data for the *NR* field in Table 11. The table also includes metallicities  $[m/H]$  for these stars that have been recomputed assuming that the interstellar component of the Ca II K-line has an equivalent width of 0.3 Å.

## C. COMPARISONS BETWEEN SURVEYS FOR BHB STARS.

### C.1. BHB Stars selected in the *B2M* Survey.

The *B2M* survey (Beers et al. 2007b) used 2MASS (*JHK*) magnitudes to derive  $V_{20}$  magnitudes and  $(B-V)_{20}$  colors for stars taken from the *HK* objective prism survey of Beers et al. (1988, 1996). The stars for which they derived  $-0.20 \leq (B-V)_{20} \leq +0.20$  were given a high (H) probability of being BHB stars. Those with  $+0.20 \leq (B-V)_{20} \leq +0.40$  were given a medium (M) probability and redder stars were assigned a low (L) probability. The *B2M* survey overlaps ~50% of the area of the *NR* survey. We measured  $V$  and  $(B-V)$  for 23 of the *B2M* stars in this area. Fig. 15(a) and 15(b) show plots of our  $V_0$  and  $(B-V)_0$  against the corresponding *B2M* values. The error of 0.14 mag that *B2M* give for their  $V_0$  magnitudes seems realistic for stars with  $V < 14.0$  but may be an underestimate for fainter stars. The error of 0.08 mag that *B2M4* quote for their  $(B-V)_{20}$  is in good agreement with the error of 0.09 mag that we estimate from the scatter in Fig. 15(b). Even so, we find that 20% to 25% of the stars for which *B2M* give  $(B-V)_{20} \leq +0.20$  are actually redder than  $(B-V)_0 = 0.20$  and so are unlikely to be BHB stars.

The *B2M* survey has 45 stars in the region of overlap with the *NR* survey. *B2M* give 26 of these stars a high probability (H) and 3 a medium probability (M) of being BHB stars. Fig 10(d) shows the  $(J-H)_0$  vs.  $(H-K)_0$  plot for the 26 stars that *B2M* consider having a high (H) probability of being BHB stars. Four of these (41, 56, 122 and 162) lie outside the defining window while the color errors of star 87 are too large for it to be selected using 2MASS colors. The remaining 17 stars (those in the sky covered by the *NR* survey but not given in Table 1) are given in Table 10 in Appendix B; they are mostly stars that are either too faint or too red to have been discovered by Rodgers et al. (1993a).

### C.2. BHB Stars selected in the *CHSS* Survey.

The Century Halo Star Survey (*CHSS*) (Brown et al. 2008) used 2MASS colors to make a preliminary selection of BHB candidates and then made a further selection using data derived from slit spectra taken with the FAST spectrograph of the Whipple 1.5-m telescope. (2.3Å resolution,  $\lambda\lambda$  3450–5450 Å). This additional use of spectra not

TABLE 11  
EQUIVALENT WIDTHS, RADIAL VELOCITIES AND METALLICITIES FOR PROGRAM STARS WITH  
 $0.00 \leq (B - V)_0 \leq 0.26$ .

No.	Object	$W_0(K)$ <sup>a</sup> Å	$W(H\delta)$ <sup>b</sup> Å	$RV_{LSR}$ <sup>c</sup> km s <sup>-1</sup>	$(B - V)_0$	[m/H] <sup>d</sup>	[m/H] <sup>e</sup>
002	Pn23l2-18	2.8	18.5	+007	0.176	-1.0	-0.8
003	Pn23s1-15	0.0	15.0	-211	-0.026	<-3.0	-2.0
004	Pn24l-37	1.7	17.2	<b>+020</b>	0.131	-1.4	-1.2
007	Pn24l-46	3.1	16.5	-074	0.245	-1.3	-1.1
010	Pn24l-47	1.1	18.3	+020	0.140	-1.9	-1.6
015	Pn24l-32	2.3	16.4	-204	0.04:	+0.0	>0.0
017	Pn23s1-2	2.6	11.6	000	0.171	-1.0	-0.8
020	Pn24l-35	2.6	15.7	-005	0.203	-1.3	-1.1
024	Pn24l-34	5.6	15.2	-026	0.192	>0.0	>0.0
027	Pn24l-48	1.6	18.3	+078	0.164	-1.6	-1.5
030	Pn24l-50	0.00	15.6	-220	-0.049	<-3.0	-2.0
034	Pn23l2-9	4.4	19.6	+003	0.237	-0.5	-0.3
037	Pn24l-49	3.1	12.9	+021	0.245	-1.3	-1.1
038	Pn24l-51	0.0	16.2	<b>-164</b>	0.039	<-3.0	-2.2
041	Pn23l2-14	0.0	19.8	<b>-270</b>	0.023	<-3.0	-2.2
048	Pn24l-45	0.9	21.5	<b>-114</b>	0.020	-1.2	-0.8
050	Pn24l-31	1.8	19.1	-089	0.155	-1.5	-1.3
052	Pn23l2-63	3.9	14.5	-154	0.246	-0.9	-0.7
053	Pn24l-30	1.3	18.1	-021	0.135	-1.7	-1.4
059	Pn24l-43	5.6	15.8	-032	0.219	>0.0	>0.0
060	Pn24l-42	0.0	20.8	<b>-208</b>	0.057	<-3.0	-2.6
063	Pn23l2-2	3.0	20.5	<b>-038</b>	0.184	-1.0	-0.7
065	Pn24l-52	3.6	21.2	+043	0.200	-0.6	-0.4
072	Pn23l2-4	3.6	19.8	<b>+009</b>	0.280	-1.2	-1.3
077	Pn24l-15	2.3	20.8	+001	0.160	-1.2	-0.9
079	Pn24l-14	0.0	13.6	+014	-0.049	<-3.0	-2.0
081	Pn24s-15	0.5	17.7	+035	0.082	-2.2	-1.8
083	Pn24l-16	1.2	25.6	-106	0.090	-1.5	-1.2
085	Pn23l2-37	2.9	22.9	-027	0.102	+0.0	+0.0
087	Pn23l2-35	0.0	19.6	-273	+0.5::	...	...
090	Pn23l2-36	0.1	15.5	<b>-020</b>	-0.062	<-3.0	-1.5
092	Pn23l1-29	1.0	20.1	-220	0.037	-1.3	-1.0
094	Pn23l2-33	2.2	8.2	-065	0.4:	...	...
095	Pn23s2-20	4.6	18.3	+002	0.191	+0.0	+0.0
099	Pn23l2-22	1.6	13.6	<b>-213</b>	0.105	-1.3	-1.0
100	Pn23s2-28	4.0	15.1	-012	0.189	-0.3	+0.0
103	Pn23s2-17	2.9	12.7	000	0.234	-1.4	-1.2
104	Pn23l2-58	0.1	17.2	-265	0.114	<-3.0	-2.7
106	Pn24l-10	3.2	17.3	+078	0.131	-0.3	+0.0
110	Pn23l2-28	0.1	19.7	<b>-054</b>	0.047	-3.0	-2.2
111	Pn24l-17	4.9	13.1	-016	0.213	+0.0	+0.0
112	Pn24s-17	4.7	13.1	-019	0.256	-0.4	-0.2
113	Pn24l-2	3.0	15.7	-093	0.213	-1.1	-0.9
115	Pn24l-55	0.3	17.8	<b>-132</b>	0.042	-2.4	-1.8
116	Pn24s-3	2.2	17.0	-009	0.193	-1.5	-1.3
120	Pn24l-56	1.8	13.4	<b>-064</b>	0.198	-1.7	-1.6
121	Pn23l2-27	1.4	22.4	-019	0.124	-1.6	-1.4
127	Pn24l-19	3.8	17.0	-091	0.250	-1.0	-0.8
128	Pn23l2-30	0.4	16.5	<b>+058</b>	0.057	-2.2	-1.8
133	Pn23l2-26	1.1	17.8	-001	0.176	-2.0	-1.8
134	Pn24l-8	3.0	15.2	<b>-126</b>	0.148	-0.6	-0.4
136	Pn24s-8	0.6	18.2	+031	0.074	-2.0	-1.6
138	Pn23s1-19	1.4	17.3	-009	0.101	-1.4	-1.2
140	Pn23l2-53	2.8	16.1	<b>-042</b>	0.265	-1.5	-1.3
141	Pn24l-22	1.9	13.8	<b>-117</b>	0.207	-1.7	-1.5
143	Pn23l2-39	1.3	15.5	+017	0.116	-1.5	-1.4
145	Pn24l-4	1.4	16.9	<b>-150</b>	0.027	-0.5	-0.2
146	Pn24l-27	2.4	19.5	<b>-049</b>	0.058	+0.0	+0.0
147	Pn23l2-25	1.4	21.8	-092	0.131	-1.6	-1.4
148	Pn24l-26	3.7	20.2	<b>-046</b>	0.089	>0.0	>0.0
151	Pn24l-6	1.3	17.8	<b>+047</b>	-0.017	0.0	>0.0
156	Pn23l-40	1.8	15.5	-098	0.299	-2.0	-1.9
157	Pn23l1-39	1.4	16.2	<b>-049</b>	0.075	-1.2	-1.0
158	Pn24l-28	4.1	19.0	+042	0.165	0.0	+0.0
161	Pn24s-23	2.5	18.1	-036	0.234	-1.5	-1.3
162	Pn24l-29	0.0	17.4	-017	0.062	<-3.0	-2.3
163	Pn23l2-43	2.3	17.0	<b>+010</b>	0.227	-1.5	-1.4
165	Pn24s-55	1.3	13.4	-159	0.246	-2.3	-2.0
168	Pn24s-60	2.8	18.5	+028	0.158	-0.8	-0.6
169	Pn23l2-45	0.2	13.9	<b>-012</b>	0.047	-3.0	-2.0

<sup>a</sup> Equivalent width of Ca II K line with 0.6 Å correction for interstellar component from Rogers et al. (1993b) Table 1.

<sup>b</sup> Equivalent width of H δ line from Rogers et al. (1993b) Table 1.

<sup>c</sup> Radial velocity corrected to LSR from Rogers et al. (1993b) Table 1 or our adopted values (boldface).

<sup>d</sup> Approximate metallicity derived from plot of  $W(K)_0$  and  $(B - V)_0$  as described in Sec. 6.1:

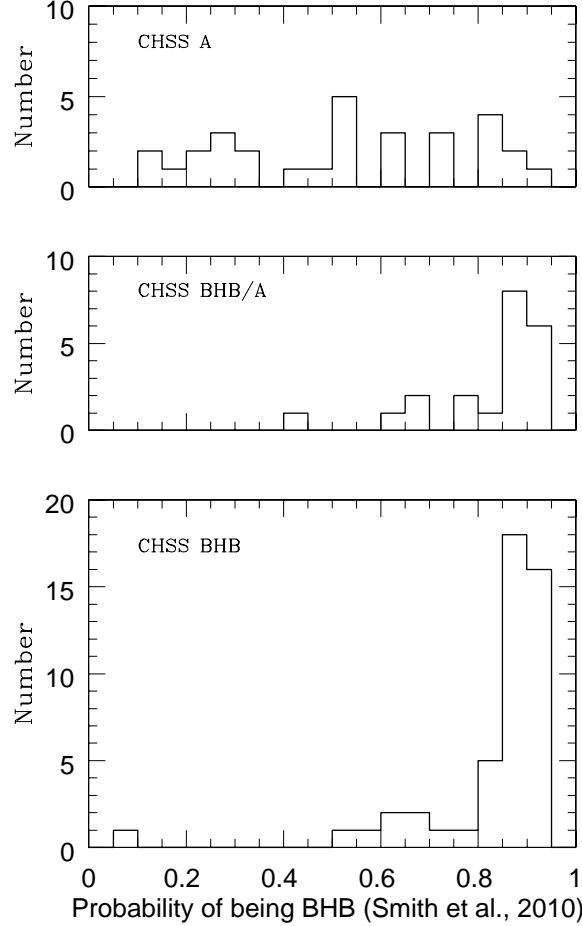


FIG. 16.— Histograms of the probabilities of a star being a BHB star according to Smith et al. (2010) for various classifications in the Century (*CHSS*) Survey: Type A (top); Type BHB/A (middle) and Type BHB (bottom).

only makes their classification much more secure than that of the *B2M* survey but also provides metallicities and radial velocities. The *CHSS* survey overlaps  $\sim 30\%$  of the *NR* field and has 12 stars in this area. Ten of these are listed in the *NR* survey and given in Table 1. Three of these (CHSS 3068, CHSS 3071 & CHSS 3075 corresponding to stars 99, 110 and 157 in the *NR*) were also classified by them as BHB stars. The other seven were classified otherwise. Of the two *CHSS* stars in the *NR* field that were not found by Rodgers et al. (1993a), CHSS 3069 is not a BHB star and CHSS 3078 is classed as a BHB star but is too faint ( $V > 15.5$ ) to be in the *NR* survey.

### C.3. BHB Stars selected by Smith et al. (2010) from DR7 of the SDSS.

DR7 intersects the *NR* field with Stripes 76 and 79 but only five of our BHB candidates are faint enough to be included in this catalog. We classify stars 99 and 110 as BHB3 (likely to be BHB stars) and Smith et al. give these relatively high probabilities of 0.756 and 0.831 of being BHB stars. We classify 63, 148 and 163 as BHB1 (unlikely to be BHB stars); these are given lower probabilities of 0.704, 0.261 and 0.123 respectively. Star 63 (for which Smith et al. give a probability of 0.704 that it is a BHB star) is CHSS 3064 and is unclassified in the *CHSS* survey.

We compare the *CHSS* and Smith et al. surveys with a sample of stars with 2MASS  $J > 15.0$ . This sample contained 99 stars for which both *CHSS* classes and Smith et al. probabilities ( $P$ ) were available. Histograms showing the distribution of Smith et al. probabilities among the *CHSS* classes are shown in Fig 16. For the BHB class, 39 stars have  $P > 0.8$  and 9 have  $P < 0.8$ . For the BHB/A class, 15 stars have  $P > 0.8$  and 6 have  $P < 0.8$ . For the A class, 7 stars have  $P > 0.8$  and 23 have  $P < 0.8$ . By taking the “cut” at  $P = 0.80$ , we maximize the agreement for both class BHB and class A; in this case we find  $\sim 80\%$  agreement between the two catalog. If we lower the “cut” to a lower  $P$  to increase the agreement with the BHB class we would include more stars that *CHSS* classify as A class (A-type stars).

We make a similar comparison with the *B2M* catalog for a sample of stars with 2MASS  $J > 15.0$ . In Fig. 17 the probability ( $P$ ) from Smith et al. is shown for these stars as a function of the SDSS color  $(g-r)_0$  with those classed H (black), H: (red) and M (green). Of these 46 stars, 21 have  $P > 0.80$  and 18 have been given  $P = 0.0$  since they are in the DR7 catalog but not in the Smith et al. catalog. Fig. 17 also shows the color distribution of a small random sample of the stars in the Smith et al. catalog that have  $P \geq 0.8$ ; they cover the range  $-0.30 \leq (g-r)_0 \leq 0.00$  (equivalent to  $-0.1 \leq (B-V)_0 \leq +0.20$ ). The *B2M* catalog BHB stars have a quite different color distribution and are all bluer than  $(g-r)_0 = -0.14$  (or  $(B-V)_0 = +0.05$ ). This confirms our earlier conclusion that many of the stars in the *B2M*

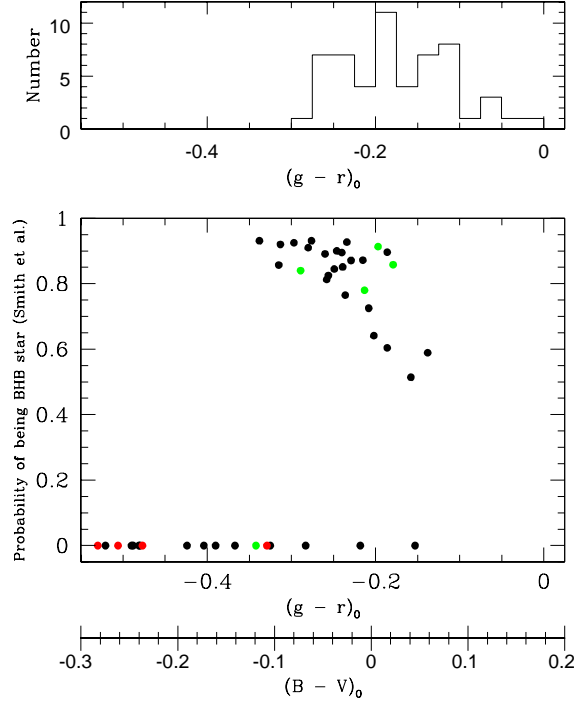


FIG. 17.— (above): Color distribution of small random sample of the stars whose probability ( $P$ ) of being a BHB star is greater than 0.8 according to Smith et al. (2010). (below): Probability  $P$  vs. color  $(g-r)_0$  for BHB stars from the B2M survey with probabilities H (black filled circles); H: (red filled circles) and M (green filled circles). B2M stars that are not in the Smith et al. catalog but are in DR7 have been given  $P = 0.0$ .

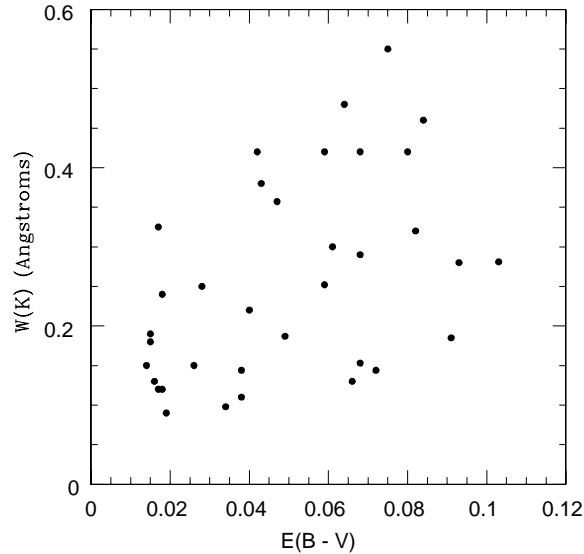


FIG. 18.— The interstellar Ca II K line equivalent width  $W(K)$ , in  $\text{\AA}$ , vs the interstellar reddening  $E(B-V)$ . The sources of the data are given in the text.

catalog with an H classification may not be BHB stars.

#### D. THE CORRECTION FOR THE INTERSTELLAR CA II K LINE.

The equivalent width  $W_0(K)$  of the Ca II K line given by Rodgers et al (1993b) used a constant correction of 0.6  $\text{\AA}$  for the interstellar component. Beers (1990) has given the following expression for the strength  $W(K)$  of the interstellar K line:

$$W(K) \sin |b| = W_{max}(1 - e^{-|z|/h}) \quad (\text{D1})$$

where  $W_{max} = 0.192 \text{ \AA}$ ,  $z$  is the height in parsecs above the plane,  $h$  is a scale height (1081 pc) and  $b$  is the galactic latitude. According to this expression, the maximum equivalent width of the interstellar K line at galactic latitude  $45^\circ$  is 0.27  $\text{\AA}$ . There are six stars in Table 1 of Beers (1990) that are in the galactic longitude range  $75^\circ$  to  $105^\circ$  and



the galactic latitude range  $-30^\circ$  to  $-60^\circ$ ; they have a mean  $W(K)$  of  $0.23 \pm 0.06 \text{ \AA}$  and a mean  $z$  of 3965 pc.

We might also expect some correlation between  $W(K)$  and the reddening  $E(B - V)$ . Fig. 18 is a plot between these quantities for stars whose height above the galactic plane is greater than 1 kpc. The  $W(K)$  are taken from Table 1 of Beers (1990) and the  $E(B - V)$  from Schlegel et al. (1998). The stars in Table 11 have  $E(B - V)$  in the range 0.04 to 0.14 with a mean value of 0.068. The correlation between  $W(K)$  and  $E(B - V)$  is too weak to make it worth computing  $W(K)$  individually for each  $E(B - V)$ . On the other hand, a mean value of  $W(K)$  of  $0.3 \text{ \AA}$  is clearly in better agreement with the reddening than the  $0.6 \text{ \AA}$  used by Rogers et al. (1993b). We therefore also computed the metallicities for the program stars using a constant  $W(K)$  of  $0.3 \text{ \AA}$  and these are given in the last column of Table 11 in Appendix B.

TABLE 1  
PHOTOMETRIC DATA FOR STARS IN THE *NR* FIELD OF RODGERS ET AL. (1993).

No. (1)	ID (2)	<i>V</i> (3)	( <i>B</i> − <i>V</i> ) (4)	( <i>u</i> − <i>B</i> ) <sub><i>K</i></sub> (5)	$\beta$ (6)	<i>E</i> ( <i>B</i> − <i>V</i> ) (7)	<i>NUV</i> (8)	<i>J</i> (9)	<i>K</i> (10)	<i>m<sub>R</sub></i> (11)	$\Sigma m_R$ (12)	No. (13)
1	Pn23l2-7	12.90±0.02	0.437±0.010	...	...	0.09	16.53	11.92	11.74	13.08	0.06	
2	Pn23l2-18	12.27±0.03	0.238±0.009	1.934±0.011	2.843±0.016	0.04	15.09	11.74	11.67	12.45	0.03	
3	Pn23s1-15	13.28±0.02	0.011±0.015	1.660±0.019	...	0.04	...	13.25	13.28	...	...	
4	Pn24l-37	13.22±0.02	0.194±0.006	2.183±0.060	2.820±0.011	0.05	16.08	12.81	12.75	13.55	0.07	
5	Pn23s1-10	11.82 <sup>a</sup>	0.35:	...	...	0.07	15.20	11.10	10.91	12.16	0.03	
6	Pn24s-32	10.63 <sup>a</sup>	0.41:	...	...	0.04	...	9.81	9.58	10.98	0.01	
7	Pn24l-46	14.55±0.01	0.348±0.025	...	...	0.09	17.74	13.75	13.51	14.74	0.14	
8	Pn23l2-17	13.23±0.01	0.402±0.017	1.930±0.011	...	0.05	16.63	12.44	12.25	13.12	0.04	
9	Pn24l-38	13.44 <sup>a</sup>	0.32:	...	...	0.05	17.08	12.77	12.61	13.53	0.07	
10	Pn24l-47	13.07±0.01	0.195±0.012	1.910±0.026	...	0.05	15.62	12.70	12.62	13.22	0.06	
11	Pn23s2-2	12.15 <sup>a</sup>	0.46:	...	...	0.08	15.88	11.21	10.98	12.41	0.04	
12	Pn23l2-19	13.58±0.01	0.334±0.045	1.730±0.039	...	0.05	16.68	13.18	12.97	14.02	0.17	
13	Pn24l-36	13.44	0.434	...	...	0.06	16.29	12.38	12.10	13.61	0.06	
14	Pn23l2-16	13.89 <sup>a</sup>	0.51:	...	...	0.04	17.39	12.92	12.62	13.94	0.07	
15	Pn24l-32	15.12±0.03	0.118±0.068	2.255±0.008	...	0.08	17.70	14.76	14.75	9.00	9.00	
16	Pn23l2-1	14.02±0.02	0.476±0.032	1.870±0.106	...	0.07	17.58	12.76	12.52	14.02	0.31	
17	Pn23s1-2	12.52±0.01	0.241±0.006	1.965±0.014	...	0.06	15.51	12.01	11.91	12.80	0.04	
18	Pn23l1-11	15.57	−0.230	...	...	0.05	...	15.54	15.22	15.33	0.20	
19	Pn23l2-6	13.84±0.03	0.447±0.021	...	...	0.07	17.44	12.82	12.57	14.02	0.08	
20	Pn24l-35	13.91±0.02	0.257±0.016	1.972±0.030	...	0.07	...	13.31	13.17	14.14	0.11	
21	Pn23s1-3	12.66 <sup>a</sup>	0.46:	...	...	0.07	16.64	11.67	11.44	12.86	0.03	
22	Pn23l2-8	14.24 <sup>a</sup>	0.33:	...	...	0.06	17.69	13.55	13.37	14.64	0.12	
23	Pn23s1-14	13.22 <sup>a</sup>	0.52:	...	...	0.04	...	12.18	11.90	13.14	0.05	
24	Pn24l-34	14.31±0.01	0.269±0.034	1.811±0.040	...	0.08	17.35	13.72	13.56	14.48	0.11	
25	Pn23s1-13	13.10 <sup>a</sup>	−0.260	...	...	0.04	...	13.82	14.08	13.77	0.08	
26	Pn24l-33	14.38±0.04	0.353±0.065	...	...	0.08	17.57	13.42	13.16	14.52	0.14	
27	Pn24l-48	12.77±0.01	0.212±0.012	1.938±0.070	...	0.05	15.55	12.31	12.17	13.12	0.04	
28	Pn24s-33	12.42±0.01	0.420±0.003	1.978±0.004	...	0.11	16.34	11.51	11.31	12.61	0.03	
29	Pn23l2-5	13.02 <sup>a</sup>	0.56:	...	...	0.05	15.91	11.91	11.60	13.22	0.04	
30	Pn24l-50	14.70±0.02	0.007±0.022	1.821±0.116	...	0.06	16.61	14.54	14.48	14.80	0.15	
31	Pn24s-31	12.69±0.02	0.423±0.011	1.752±0.042	...	0.06	16.47	11.81	11.58	12.76	0.06	
32	Pn23l2-20	14.10 <sup>a</sup>	0.66:	...	...	0.04	...	12.98	12.55	13.97	0.09	
33	Pn23s1-4	11.11±0.04	0.348±0.003	1.912±0.020	2.755±0.010	0.05	14.70	10.40	10.24	11.43	0.02	
34	Pn23l2-9	13.38±0.02	0.313±0.015	2.040±0.014	...	0.08	16.88	12.74	12.58	13.58	0.06	
35	Pn24s-30	11.95±0.01	0.408±0.002	...	...	0.07	...	11.13	10.93	12.12	0.02	
36	Pn24s-37	11.92±0.01	0.398±0.006	...	...	0.08	...	11.15	10.95	11.50	0.04	
37	Pn24l-49	11.54±0.01	0.298±0.006	...	...	0.05	14.65	11.17	11.03	11.96	0.14	
38	Pn24l-51	12.93±0.01	0.103±0.004	2.147±0.036	2.850±0.024	0.06	15.44	12.60	12.53	12.90	0.04	
39	Pn24l-41	12.33 <sup>a</sup>	0.43:	...	...	0.10	15.85	11.41	11.20	12.55	0.04	
40	Pn23s2-9	11.76±0.01	0.330±0.006	1.973±0.003	...	0.05	15.35	11.09	10.98	12.09	0.02	
41	Pn23l2-14	14.44±0.01	0.072±0.015	2.070±0.059	...	0.05	16.68	14.15	14.09	14.73	0.13	
42	Pn24s-35	12.18±0.01	0.418±0.006	...	...	0.09	15.97	11.35	11.15	12.48	0.03	
43	Pn24s-29	11.23 <sup>a</sup>	0.28:	...	2.816±0.010	0.07	...	10.50	10.40	11.60	0.02	
44	Pn23l2-69	13.52 <sup>a</sup>	0.41:	...	...	0.06	16.78	12.65	12.43	13.52	0.05	
45	Pn24s-40	11.28 <sup>a</sup>	0.36:	...	2.761±0.010	0.08	14.63	10.53	10.34	11.43	0.04	
46	Pn23s2-10	10.59 <sup>a</sup>	0.32:	...	2.742±0.005	0.05	14.12	9.90	9.74	10.96	0.02	
47	Pn23s2-48	12.42 <sup>a</sup>	0.52:	...	...	0.05	15.98	11.32	11.06	12.68	0.12	
48	Pn24l-45	14.63±0.01	0.085±0.004	2.154±0.078	...	0.06	...	14.37	14.40	...	...	
49	Pn23s2-11	10.41±0.01	0.316±0.002	1.858±0.007	2.768±0.008	0.04	...	9.74	9.59	10.77	0.02	
50	Pn24l-31	13.05±0.03	0.225±0.021	1.878±0.030	...	0.07	15.49	12.54	12.37	13.35	0.07	
51	Pn23l2-13	13.14 <sup>a</sup>	0.54:	...	...	0.05	16.23	12.04	11.75	13.27	0.06	
52	Pn23l2-63	14.19±0.04	0.288±0.030	1.705±0.040	...	0.04	16.89	13.53	13.35	14.60	0.13	
53	Pn24l-30	13.82 <sup>a</sup>	0.189±0.009	2.013±0.050	...	0.07	16.70	13.37	13.29	14.14	0.09	
54	Pn23l2-10	13.36 <sup>a</sup>	0.53:	...	...	0.05	16.78	12.41	12.08	13.58	0.07	
55	Pn23l2-11	14.95 <sup>b</sup>	0.6:	...	...	0.04	18.58	13.94	13.56	15.36	0.16	
56	Pn24l-44	13.75	−0.175	...	...	0.09	...	14.14	14.36	13.34	0.07	
57	Pn23s2-13	12.70 <sup>a</sup>	0.44:	...	...	0.04	16.27	11.78	11.56	12.87	0.03	
58	Pn24s-26	14.16 <sup>a</sup>	0.45:	...	...	0.14	...	13.33	13.05	14.33	0.11	
59	Pn24l-43	14.55±0.01	0.288±0.009	1.955±0.040	...	0.07	17.89	13.95	13.71	15.03	0.17	
60	Pn24l-42	14.84±0.03	0.127±0.34	2.240±0.051	...	0.07	17.67	14.32	14.09	15.31	0.20	

NOTE. — Only a portion of this table is shown here to demonstrate its form and content. The full table is available in the published paper.

<sup>a</sup> Magnitude from *ASAS* − 3 catalog.

<sup>b</sup> Magnitude from *ASAS* − 3 and *GSC* − 2.3 catalogs.

(1) Variable. See Table 2.

(2) RR Lyrae variable IX PEG. See Table 2.

(3) Subdwarf KUV 23089+0942. *BV* from Wegner et al. (1990).

(4) White Dwarf PG2309+105. *BV* from Eggen (1968).

(5) Variable. See Table 2.

(6) Variable. See Table 2.

(7) Subdwarf PG2314+076. *BV* from Allard et al. (1994).